Ice age True Polar Wander in a compressible and non-hydrostatic Earth

Gabriele Cambiotti,[1] Yanick Ricard[2] and Roberto Sabadini[1]

[1]*Department of Earth Science, University of Milan, Milan, Italy. E-mail: cambiottigabriele@hotmail.it*
[2]*Laboratoire des Sciences de la Terre, CNRS, Unviersité de Lyon 1, ENSL, Lyon, France*

SUMMARY

Issues related to long timescale instability in the Earth's rotation, named True Polar Wander (TPW), have continuously been debated, after the pioneering works of the sixties. We show ice age TPW results from a newly developed compressible model, based on the numerical integration in the radial variable of the momentum and Poisson equations and on the contour integration in the Laplace domain which allows us to deal with the non-modal contribution from continuous radial rheological variations. We thus fully exploit the long term behaviour of the Earth's rotation and we quantify the effects of the compressible rheology, compared to the widely used incompressible one. We discuss the so-called 'traditional approach' to the Earth's rotation developed during the eighties and nineties, both for ice age and mantle convection TPW and we explain within this approach the sensitivity of TWP predictions to the elastic and viscoelastic rheologies of the lithosphere. We agree on the necessity to include the effects of the non-hydrostatic bulge from mantle convection to obtain realistic ice age TPW rates in the lower mantle viscosity range $[10^{21}, 10^{22}]$ Pa s, as first indicated by Mitrovica *et al*. Their analysis represents a first attempt to couple the effects on TPW from mantle convection and glacial forcing, by including the non-hydrostatic bulge due to mantle convection but not the other time-dependent driving terms. This partial coupling freezes in space the non-hydrostatic contribution due to mantle convection, thus damping the present-day ice age TPW and forcing the axis of instantaneous rotation to come back to its initial position when ice ages started as discussed in Mitrovica *et al*. We also describe a peculiar behavior of the new ice age TPW predictions exhibiting a dampened pendulum motion, with the axis of instantaneous rotation overcrossing the position it had before ice ages started. We argue that a viscoelastic rather than elastic lithosphere should be adopted in the modelling of TPW although, on the time of ice ages, it is difficult to disentangle the effects of lithospheric rheology and of mantle convection. We discuss the implication of self-consistent convection calculations of the non-hydrostatic contribution and its impact on the long term Earth's rotation stability during ice ages. The ice age TPW cannot account for more than 70 per cent of the observed one, at least for lower mantle viscosities lower than 10^{22} Pa s: mantle convection must therefore contribute to the observed TPW.

Key words: Earth rotation variations; Dynamics of lithosphere and mantle; Rheology: mantle.

1 INTRODUCTION

Starting from the work by Munk, MacDonald and Gold, issues related to the secular change of the Earth's rotation axis named True Polar Wander (TPW), never ceased to be discussed or questioned. Progress has been made since the sixties, on two major aspects: the first deals with the improvement in the modelling of the Earth, in terms of rheological stratifications, and the second is related to the new insights on surface and deep seated density anomalies originating from ice ages and mantle convection as major sources

of polar wander. After decades, we are however still in the situation in which it is necessary to come back to some basic TPW issues to dig out deeper insights into the physics of this aspect of the dynamics of our planet, focusing, in particular, on the nature, elastic or viscoelastic, of the outermost part of our planet.

Ricard *et al*. (1993b) first exploited the rotational behaviour of elastic versus viscoelastic outermost part of the Earth, introducing the T_1 timescale characterizing the readjustment of the equatorial bulge, based on a realistically stratified viscoelastic Earth models. Vermeersen & Sabadini (1999) pointed out the reduction in

the TPW displacements for Maxwell Earth models carrying a viscoelastic lithosphere compared to those with an elastic one. Nakada (2002) went thoroughly into the issue related to the rheology of the lithosphere by considering highly viscous viscoelastic lithospheres and he showed as the TPW rates in the lower mantle viscosity range $[10^{21}, 10^{22}]$ Pa s are extremely sensitive to the choice of the rheology of the lithosphere, elastic or viscoelastic with high viscosity. This might be seen as surprising since the highly viscous viscoelastic lithosphere is expected to behave as an elastic one for timescales of 1 Myr comparable to that of postglacial rebound. Mitrovica *et al.* (2005) named this sensitivity of the TPW predictions the 'Nakada paradox' and (as cited by Nakada) 'has suggested that this paradox originates from an inaccuracy in the traditional rotation theory associated with the treatment of the background equilibrium rotating form upon which any load- and rotation-induced perturbations are superimposed (e.g. Wu & Peltier 1984)'.

Starting from these preliminary remarks, Mitrovica *et al.* (2005) suggest a new treatment of the rotational dynamics where the observed fluid Love number is used in the linearized Euler dynamic equation, rather than the tidal fluid limit deduced self-consistently from the Maxwell Earth model used to evaluate the load-induced perturbations of the inertia tensor and the readjustment of the equatorial bulge. This apparently minor change (the discrepancy between the observed and tidal fluid limits is about 1 per cent) has a potentially large impact on TPW predictions and would solve the 'Nakada paradox'.

In this paper, we will restate the mathematical framework of the linearized Earth's rotation theory in order to enlighten the differences between the so-called 'traditional approach' (Sabadini & Peltier 1981; Sabadini *et al.* 1982; Wu & Peltier 1984) and the treatment indicated by Mitrovica *et al.* (2005). We will show results from a newly developed compressible model, including the methodology to transform the results from the Laplace domain into the time domain. This will clarify some issues related to the use of the normal mode relaxation approach within rotational problems. We will explore the role of the non-hydrostatic contribution to the fluid Love number from mantle convection calculations in order to make our estimates of TPW rates, within the scheme proposed by Mitrovica *et al.* (2005), as realistic as possible.

2 MATHEMATICAL FORMALISM

The equation of motion of a rotating body in a rotating frame is the well-known Euler dynamic equation. When no external torque is applied, it reads

$$\frac{d\,(\mathbf{J} \cdot \boldsymbol{\omega})}{dt} + \boldsymbol{\omega} \times (\mathbf{J} \cdot \boldsymbol{\omega}) = \mathbf{0} \tag{1}$$

with $\mathbf{J}$ and $\boldsymbol{\omega}$ being the inertia tensor and the angular velocity. Before any perturbation occurs we consider the Earth rotating with constant angular velocity $\boldsymbol{\omega}(t \leq 0) = (0, 0, \Omega)$, oriented along the z-axis, and we write $\boldsymbol{\omega}(t > 0)$ in the perturbed state in terms of its direction cosines m_1 and m_2, with respect to the axes x and y, and of the relative variation of the diurnal rotation rate m_3

$$\boldsymbol{\omega} = \Omega(m_1, m_2, 1 + m_3). \tag{2}$$

Let us subdivide the inertia tensor into two parts

$$\mathbf{J} = \mathbf{J}^\omega + \mathbf{J}^L \tag{3}$$

the first, $\mathbf{J}^\omega$, describing the inertia tensor of the spherically symmetric Earth model plus the effects of the centrifugal potential and

the second, $\mathbf{J}^L$, describing the remaining contributions, from ice age loading and mantle convection.

The difference between the approach used in a series of papers (Sabadini & Peltier 1981; Sabadini *et al.* 1982; Wu & Peltier 1984) and the newly proposed on by Mitrovica *et al.* (2005) can be appreciated by starting from MacCullagh's formula (Jeffreys 1952; eq. 5.2.3 of Munk & MacDonald 1960)

$$J_{ij}^\omega = I\,\delta_{ij} + \frac{a^5}{3\,G}\,k^T \star \left(\omega_i\,\omega_j - \frac{1}{3}\omega^2\,\delta_{ij}\right) \tag{4}$$

where $\star$ stands for the convolution operator. The I, a, G and k^T are the inertia moment, the radius of the spherically symmetric Earth model, the Gravitational constant and the degree-2 tidal gravitational Love number in the time t-domain. By assuming that the Earth has reached its rotating equilibrium state with the constant angular velocity before the beginning of the ice ages, $\boldsymbol{\omega} = (0, 0, \Omega)$, we get

$$\mathbf{J}^\omega(t = 0) = \mathrm{Diag}\,[A, A, C] \tag{5}$$

with $\mathrm{Diag}\,[\ldots]$, C and A denoting the 3×3 diagonal matrix and the equilibrium polar and equatorial inertia moments given by

$$C = \frac{2}{3}\frac{a^5\,\Omega^2}{3\,G}\,k_F^T \qquad A = -\frac{1}{3}\frac{a^5\,\Omega^2}{3\,G}\,k_F^T \tag{6}$$

as it results from MacCullagh's formula (4) for $\boldsymbol{\omega} = (0, 0, \Omega)$, with k_F^T being the tidal gravitational fluid limit of the Maxwell model. This latter is defined as the limit for $t \to \infty$ of the convolution of the degree-2 tidal gravitational Love number k^T with the Heaviside time history $H(t)$

$$k_F^T = \lim_{t \to \infty} k^T(t) \star H(t). \tag{7}$$

Note that the word 'fluid' is poorly chosen when some layers are purely elastic and cannot relax their stresses. It would be less confusing to use the expression tidal 'equilibrium' limit (Mitrovica *et al.* 2005). It is only to be in agreement with all our predecessors that we keep the inaccurate but widely used term of tidal 'fluid' limit.

Eq. (5) using eqs (6) and (7) implies that before the ice load perturbation, the Earth was submitted to a constant rotation for a timescale greater than the longest characteristic relaxation Maxwell time of all the viscoelastic layers. Particularly, in the case of a viscoelastic lithosphere, this timescale is greater than the ice age timescale of 1 Myr for a 120 km thick viscoelastic lithosphere with viscosity ν_L higher than 10^{24} Pa s and rigidity volume averaged from PREM (Dziewonski & Anderson 1981). This shows that the theory, based on eq. (5) to estimate the initial state of rotational equilibrium, with C and A given by eq. (6), is used also on a timescale in which the elastic and the highly viscous viscoelastic lithosphere are distinguishable (see for instance Fig. 1(a) in Wu & Peltier 1982).

In the perspective of studying the ice age TPW by means of compressible Maxwell Earth models based on PREM, some remarks on the tidal fluid limit k_F^T are required. Indeed PREM has an unstable compositional stratification above the 670 km discontinuity (Plag & Jüttner 1995) corresponding to an imaginary Brunt-Väisälä frequency (i.e. the radial density increases with depth less than what should be expected from the self-compression of the mantle). This unstable stratification generates growing modes which do not converge for $t \to \infty$ in eq. (7). These modes similar to Rayleigh Taylor instabilities are discussed in various papers, as RT-modes in Plag & Jüttner (1995), Vermeersen *et al.* (1996) and Vermeersen & Mitrovica (2000) and included in the wider class of compositional C-modes in Cambiotti & Sabadini (2010). As shown in Vermeersen
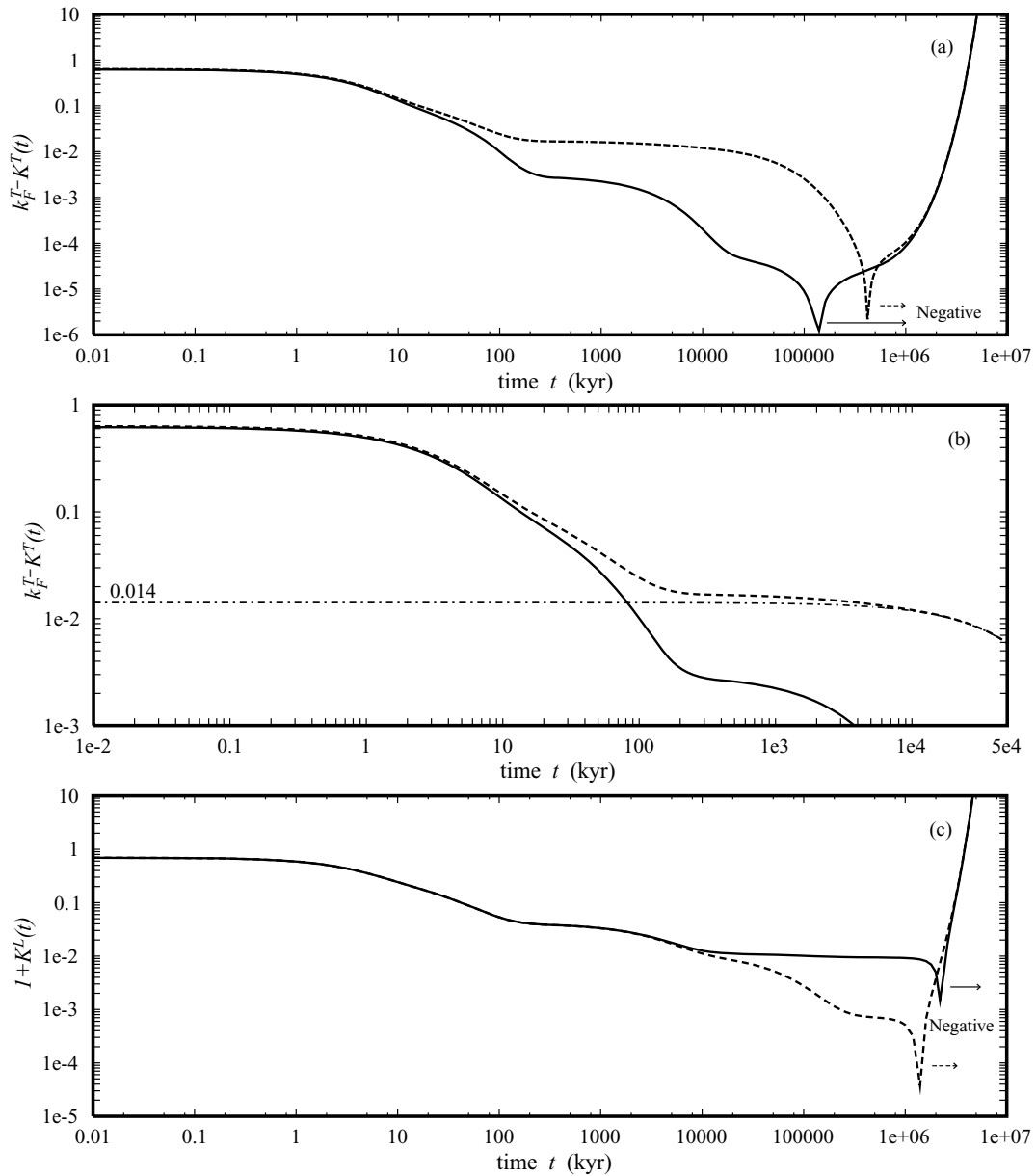
Figure 1. The readjustment of the equatorial bulge $k_T^F - K^T(t)$ (a, b) and the load response $1 + K^L(t)$ (c) for the elastic (solid) and highly viscous viscoelastic (dashed) compressible PREM, with lower mantle viscosity $\nu_{LM} = 10^{22}$ Pa s. In the panel (b) the difference between the readjustments of the equatorial bulge of the model with the elastic (E) and viscoelastic (V) lithosphere is also shown, $k_{F,V}^T - K_V^T(t) - (k_{F,E}^T - K_E^T(t))$ (dashed-dot line).

& Mitrovica (2000) these modes are characterized by long relaxation times of 10^2–10^3 Myr and thus their effects are negligible on the timescale of the ice ages. To avoid these modes, following Chinnery (1975), we compute the tidal fluid limit k_F^T by considering the viscoelastic layers of the Maxwell Earth model as inviscid, with the exception of the layers properly elastic. This approach is in agreement with the theory of the equilibrium figure of the rotating Earth at first-order accuracy and it does not differ from the assumption that Maxwell Earth models are in hydrostatic equilibrium before the loading of the last ice age, as usually done in postglacial rebound studies.

Besides this, note that we have defined k_F^T in the time t-domain. This is due to the fact that it is not possible to use its alternative definition in terms of the limit $s \to 0$ of the tidal gravitational Love number $\tilde{k}^T(s)$ in the Laplace s-domain. Indeed the origin $s = 0$ of

the Laplace s-domain is the cluster point of the denumerable set of the poles of the C-modes, both for stable and unstable compositional stratifications (Cambiotti & Sabadini 2010).

Having clarified the issues related to the tidal fluid limit k_F^T, we can write the MacCullagh's formula (4) as

$$\mathbf{J}^\omega = \text{Diag}\,[A, A, C] + \mathbf{\Delta I}^\omega \qquad (8)$$

with $\mathbf{\Delta I}^\omega$ describing the readjustment of the rotational equatorial bulge. Particularly, the perturbation in the off-diagonal components ΔI_{13}^ω and ΔI_{23}^ω results into

$$\Delta I_{j3}^\omega = \frac{a^5\,\Omega^2}{3\,G} k^T(t) \star m_j(t)\,(1 + m_3(t)) \qquad j = 1, 2 \qquad (9)$$

as in eqs (3.34) and (3.35) of Sabadini & Vermeersen (2004). In addition to this perturbation of the inertia tensor $\mathbf{J}$, one must add the

driving perturbations due to the direct effect of the ice load, $\mathbf{\Delta I}^{ice}$, and to the relevant response of the Earth, controlled by the degree-2 load gravitational Love number $k^L(t)$

$$\mathbf{J}^L = \left(\delta(t) + k^L(t)\right) \star \mathbf{\Delta I}^{ice}(t) \tag{10}$$

with $\delta(t)$ being the Dirac distribution. Then, by using eqs (2) and (3), together with eqs (8)–(10), the Euler dynamic eq. (1) can be linearized within the assumption of $m_j \ll 1$ as in eqs (3.12) and (3.13) of Sabadini & Vermeersen (2004)

$$A\,\Omega\,d_t m_1 + (C - A)\,\Omega^2\,m_2 = \Omega^2\,\Delta I_{23}^\omega + \Omega^2\,(\delta(t) + k_L) \star \Delta I_{23}^{ice}, \tag{11}$$

$$A\,\Omega\,d_t m_2 - (C - A)\,\Omega^2\,m_1 = -\Omega^2\,\Delta I_{13}^\omega$$
$$- \Omega^2\,(\delta(t) + k_L) \star \Delta I_{13}^{ice}. \tag{12}$$

For the sake of simplicity, in eqs (11) and (12) we have neglected the time derivative of the off-diagonal perturbations of the inertia tensor in view of their negligible impact on the ice age TPW. Furthermore, in the present work we do not consider the third component of the Euler dynamic eq. (1), pertaining to the relative variation in the diurnal rate m_3.

At this stage, by dividing each member of eqs (11) and (12) by $(C - A)\,\Omega^2$, we obtain

$$\frac{A}{\Omega\,(C - A)}\,d_t m_1 + m_2 = \frac{a^5\,\Omega^2}{3\,G\,(C - A)}\,k^T \star m_2$$
$$+ \frac{1}{C - A}\,(\delta(t) + k_L) \star \Delta I_{23}^{ice}, \tag{13}$$

$$\frac{A}{\Omega\,(C - A)}\,d_t m_2 - m_1 = -\frac{a^5\,\Omega^2}{3\,G\,(C - A)}\,k^T \star m_1$$
$$- \frac{1}{C - A}\,(\delta(t) + k_L) \star \Delta I_{13}^{ice}, \tag{14}$$

where the factor multiplying $k^T \star m_j$, with $j = 1, 2$, is just the inverse of the tidal fluid limit k_F^T according to eq. (6)

$$k_F^T = \frac{3\,G\,(C - A)}{a^5\,\Omega^2} \tag{15}$$

After the Laplace transformation, eqs (13) and (14) can be recast in the widely used and more compact form

$$\frac{i\,s}{\sigma_r}\,\tilde{\mathbf{m}}(s) + \left(1 - \frac{\tilde{k}^T(s)}{k_F^T}\right)\,\tilde{\mathbf{m}}(s) = \left(1 + \tilde{k}_L(s)\right)\,\tilde{\boldsymbol{\phi}}(s), \tag{16}$$

where i and σ_r are the imaginary number and the Eulerian free precession frequency

$$\sigma_r = \Omega\,(C - A)/A \tag{17}$$

and we have made use of the complex notation

$$\tilde{\mathbf{m}}(s) = \tilde{m}_1(s) + i\,\tilde{m}_2(s)$$
$$\tilde{\boldsymbol{\phi}}(s) = \frac{1}{C - A}\,\left(\tilde{\Delta I}_{13}^{ice}(s) + i\,\tilde{\Delta I}_{23}^{ice}(s)\right). \tag{18}$$

The tilde stands for the Laplace transform. This demonstrates that the theory (Sabadini & Peltier 1981; Sabadini et al. 1982; Wu & Peltier 1984), building on the work of Munk & MacDonald (1960), provides a mathematically sound treatment of ice age TPW under the assumption that the responses to the load and the equilibrium background form can be computed using the same Earth model. In this regard, different tidal fluid limits k_F^T are used in eq. (16) for

models with an elastic or viscoelastic lithosphere since the first carries a finite strength after rotational spin-up of the model, while the second is fully relaxed (Mitrovica et al. 2005). For models sharing the same reference density profile, this results in a smaller initial rotational bulge for the elastic case (E) than for the viscoelastic case (V)

$$k_{F,E}^T < k_{F,V}^T. \tag{19}$$

Two rheological models of the Earth will only predict the same ice age TPW if their behaviours agree both on the timescale of the ice ages ($\lesssim 1$ Myr) and at infinite time, since the latter controls the initial rotational bulge within the traditional approach, as shown in eq. (15). The behaviour of elastic and highly viscous viscoelastic lithospheres are indistinguishable on short timescale but not at infinite time. This issue was discussed in detail by Mitrovica et al. (2005), though we believe their use of the term 'Nakada paradox' was an overstatement. Indeed, the findings of Nakada (2002) consist in the understanding that the dependence of ice age TPW predictions on the lithospheric rheology can be very important for lower mantle viscosities lesser than 10^{22} Pa s, as we will show in detail in Sections 6 and 7.

The new treatment made by Mitrovica et al. (2005) consists in noticing that the inertia tensor of the real Earth is not only that of a laterally homogeneous rotating planet plus an ice load perturbation as implied by eq. (3), but perturbations due to the mantle 3-D structure are also present. Coming back to the stage before the linearization of the Euler dynamic eq. (1), this is equivalent to adding to the equilibrium inertia tensor obtained by the rotational spin-up of the model, eq. (5), the perturbations ΔI_{11}^C, ΔI_{22}^C and ΔI_{33}^C in the diagonal components due to mantle convection. This choice implies that mantle convection does not directly drive polar motion, since the off-diagonal components ΔI_{13}^C and ΔI_{23}^C due to mantle convection are not added, or, alternatively, that the axis of rotation has already readjusted to the slowly evolving convection forcing so that the off-diagonal inertia perturbations are only those arising from postglacial rebound. This assumption implies that the evolution of the convective mantle is so slow that it appears frozen during the glaciation–deglaciation phases. Since the series of eight ice age cycles occurs over 800 kyr, this remains probably a reasonable approximation but not necessarily so and convection may also have contributed to the TPW during this period. According to Besse & Courtillot (1991), over geological times, the TPW occurs indeed at rates not much slower than those due to glacial readjustments. This suggests that the two processes of mantle driven and surface driven TPW may be intermingled. Before Mitrovica et al. (2005), in all studies of glaciation induced TPW, the diagonal components ΔI_{11}^C, ΔI_{22}^C and ΔI_{33}^C were not introduced and the mantle was considered without lateral density variations. The role of mantle convection was studied separately from the ice age TPW, as done by Ricard et al. (1993a,b).

By keeping the assumption of symmetry around the polar axis, $\Delta I_{11}^C = \Delta I_{22}^C$, we therefore perform the change of variables

$$C \to C + \Delta I_{33}^C \qquad A \to A + \frac{\Delta I_{11}^C + \Delta I_{22}^C}{2}. \tag{20}$$

Particularly, eq. (15) has to be written as

$$k_{F,obs}^T = k_F^T + \beta = \frac{3\,G\,(C - A)}{a^5 \Omega^2} \tag{21}$$

with $k_{F,obs}^{T}$ being the observed fluid Love number and

$$\beta = \frac{3\,G}{a^5 \Omega^2}\left(\Delta I_{33}^{C} - \frac{\Delta I_{11}^{C} + \Delta I_{22}^{C}}{2}\right) \tag{22}$$

to which we refer as the β correction to the tidal fluid limit k_F^{T} following eq. (16) in Mitrovica *et al.* (2005). The $k_{F\,obs}^{T}$ is thus an observation and k_F^{T} a prediction from viscoelastic modelling, while β is the contribution of mantle convection, assumed frozen during the period of ice age TPW. In view of this, eq. (16) becomes

$$\frac{i\,s}{\sigma_r}\,\tilde{\mathbf{m}}(s) + \left(1 - \frac{\tilde{k}^{T}(s)}{k_F^{T}+\beta}\right)\tilde{\mathbf{m}}(s) = (1 + \tilde{k}_L(s))\,\tilde{\boldsymbol{\phi}}(s). \tag{23}$$

Making use of $k_{F\,obs}^{T} = k_F^{T} + \beta$, rather than k_F^{T}, has thus the meaning of coupling, in a simplified fashion and within a linearized scheme, the effects of the ice age TPW with those from mantle convection, but assuming for the latter only its contribution to the non-hydrostatic ellipsoidal shape of the Earth (ΔI_{11}^{C}, ΔI_{22}^{C} and ΔI_{33}^{C} differing from zero) and not its active driving effect (ΔI_{13}^{C}, ΔI_{23}^{C} assumed equal to zero).

For layered incompressible models it is possible to show analytically how the β correction impacts the linearized equation for the ice age TPW. The normal mode expansions for the gravitational Love numbers in the Laplace s-domain, both for loading (L) and tidal (T) forcing, is

$$\tilde{k}(s) = k_E + \sum \frac{k_j}{s - s_j} \tag{24}$$

with k_E, k_j and s_j being the elastic gravitational Love number, the residues and the poles of the j-th relaxation mode. The long term behaviour, when $s = 0$, is controlled by

$$k_F = k_E - \sum \frac{k_j}{s_j} \tag{25}$$

and therefore $\tilde{k}(s)$ can be rearranged as follows

$$\tilde{k}(s) = k_F + s \sum \frac{k_j}{s_j\,(s - s_j)}. \tag{26}$$

This allows us to collect in eq. (16) (i.e. in the case $\beta = 0$ where the initial flattening is only due to rotation without contribution from mantle dynamics) a term linear in the Laplace variable s

$$s\left(\frac{i}{\sigma_r} - \frac{1}{k_F^{T}}\sum \frac{k_j^{T}}{s_j\,(s - s_j)}\right)\tilde{\mathbf{m}}(s)$$
$$= \left(1 + k_F^{L} + s \sum \frac{k_j^{L}}{s_j\,(s - s_j)}\right)\tilde{\boldsymbol{\phi}}(s) \tag{27}$$

as in eq. (3.47) in Sabadini & Vermeersen (2004). By solving this equation for $\tilde{\mathbf{m}}(s)$, we get

$$\tilde{\mathbf{m}}(s) = \frac{1 + k_F^{L} + s \sum \frac{k_j^{L}}{s_j(s-s_j)}}{s\left(\frac{i}{\sigma_r} - \frac{1}{k_F^{T}}\sum \frac{k_j^{T}}{s_j(s-s_j)}\right)}\,\tilde{\boldsymbol{\phi}}(s), \tag{28}$$

where the factor s collected at the denominator is responsible for the so-called secular term, which characterizes the ice age TPW in such a way that it gains a net displacement at the end of each ice age cycle.

If now we want to account for the contribution of mantle convection to the inertia tensor by applying the β correction, eq. (28)

becomes

$$\tilde{\mathbf{m}}(s) = \frac{1 + k_F^{L} + s \sum \frac{k_j^{L}}{s_j(s-s_j)}}{\frac{\beta}{k_F^{T}+\beta} + s\left(\frac{i}{\sigma_r} - \frac{1}{k_F^{T}+\beta}\sum \frac{k_j^{T}}{s_j(s-s_j)}\right)}\,\tilde{\boldsymbol{\phi}}(s). \tag{29}$$

The secular term is, in this case, substituted by an extra exponential decaying term, which drags the equatorial bulge and forces the ice age TPW to return to the initial position of the rotation axis, after a sufficiently long time. This can be explained in the following way. While the hydrostatic flattening readjusts during the ice age TPW, the mantle density anomalies act as a counterweight that limits the polar excursion and ultimately control the position of the pole (fig. 14 of Mitrovica *et al.* 2005). In Section 7, we will show that these considerations are not restricted to the simple layered incompressible models, but they extend also to the case of more realistic compressible models which take into account the continuous variations of the material parameters. It is noteworthy that our advanced Earth models have a continuous relaxation spectrum (Fang & Hager 1995; Tanaka *et al.* 2006; Cambiotti & Sabadini 2010), which does not allow the analytical derivation of eqs (28) and (29) based on the discretized normal mode expansion given by eq. (24).

3 THE 1-D COMPRESSIBLE MODEL

We now consider a compressible, self-gravitating, spherically symmetric Maxwell Earth model, with the initial density $\rho^{(0)}$ and the elastic shear, μ, and bulk, κ, moduli of PREM. We consider these material parameters as given in Table 1 of Dziewonski & Anderson (1981), in terms of polynomials of the radial distance from the Earth centre r in each of the main layers of the Earth. This way we take into account the continuous variations of the material parameters, without introducing any fine layered stratification. As concerns the viscosity ν, even though we could consider continuous variations, in the present work we adopt a simple stepwise profile characterized by the lower, ν_{LM}, and upper, ν_{UM}, mantle viscosities and the lithospheric viscosity ν_L. The thickness of the lithosphere is of 120 km and we choose the lithospheric viscosity $\nu_L = 10^{26}$ Pa s to discuss the issues raised by Nakada (2002) and Mitrovica *et al.* (2005). Beside this, we consider the lower mantle viscosity ν_{LM} as free parameter, ranging from 10^{21} to 10^{23} Pa s, while the upper-mantle viscosity ν_{UM} is fixed at 10^{21} Pa s. The outer oceanic layer of PREM is replaced by extending the upper crust to the Earth's radius a. The tidal fluid limit k_F^{T} for this model with viscoelastic lithosphere agrees with the value of 0.934 given in Mitrovica *et al.* (2005).

To get the degree-n load Love number, $\tilde{\mathbf{k}}_L(n, s)$ and the tidal Love number, $\tilde{\mathbf{k}}_T(n, s)$, in the Laplace s-domain, we integrate the differential system describing the conservation of the momentum and the self-gravitation after expansion in spherical harmonics and Laplace transformation (eq. 5 in Cambiotti & Sabadini 2010). The radial integration, from the core–mantle interface r_C to the Earth surface a, is based on the Gill–Runge–Kutta fourth-order method. We consider the core as inviscid and we impose the fluid–solid boundary conditions (Chinnery 1975) as Cauchy data for the differential system at the radius r_C. This implies that we have to get the perturbation of the equipotential surface of the inviscid core at r_C and we do it as described in Smylie & Manshina (1971). At the interfaces at which the material parameters of PREM have stepwise discontinuities, we impose the material boundary conditions, while at the Earth surface a we impose the boundary conditions describing the loading and the tidal forcing (eqs 11 and 13 in Cambiotti & Sabadini 2010).

In this way, we have a numerical algorithm able to provide $\tilde{\mathbf{k}}_L(n,s)$ and $\tilde{\mathbf{k}}_T(n,s)$ at fixed Laplace variable s. As pointed out in a series of papers (Fang & Hager 1995; Tanaka *et al.* 2006; Cambiotti & Sabadini 2010), the continuous variations of the rheological parameters (not those of the initial density $\rho^{(0)}$ as pointed out in Cambiotti & Sabadini (2010) lead to a continuous relaxation spectrum and so, to get the perturbations in the time domain, we cannot resort to the normal mode approach (Wu & Peltier 1982; Han & Wahr 1995). Following the Bromwich path approach described in Tanaka *et al.* (2006), we get the degree-n non-dimensional perturbation $\mathbf{K}\,(f;n,t)$ due to a forcing with time history $f(t)$ by evaluating the following contour integral

$$\mathbf{K}(f;n,t) = \mathcal{L}^{-1}[\tilde{\mathbf{k}}(n,s)\,f(s)] = \frac{1}{2\pi i}\int_{\gamma}\tilde{\mathbf{k}}(n,s)\,\tilde{f}(s)\,e^{st}\,ds \tag{30}$$

with $\tilde{f}(s)$ being the Laplace transform of the forcing time history $f(t)$ and γ the contour in the Laplace s-domain enclosing the set $\mathcal{S}\subset\mathbb{C}$ in which $\tilde{\mathbf{k}}(n,s)$ and $f(s)$ are not analytic. We discuss the definition of the contour γ in the Appendix A.

The same algorithm is used to evaluate the direction cosines $m_1(t)$ and $m_2(t)$ describing the ice age TPW. We solve eq. (23) for $\tilde{\mathbf{m}}(s)$ and we evaluate the contour integral

$$\mathbf{m}(t) = \frac{1}{2\pi i}\int_{\gamma}\frac{1+\tilde{k}_L(s)}{1-\frac{\tilde{k}^T(s)}{k_F^T+\beta}}\,\tilde{\boldsymbol{\phi}}(s)\,e^{st}\,ds. \tag{31}$$

Note that, we have made use of the approximation proposed in Wu & Peltier (1984), which consists in neglecting in eq. (23) the term associated with the Eulerian free precision σ_r. As pointed out in Mitrovica & Milne (1998), this replaces the Chandler wobble by an instantaneous elastic response, representing the time average of the Chandler Wobble. In this way, we can maintain the same contour γ as in eq. (30) since the rotation pole associated with the Chandler Wobble is avoided (this pole with a large imaginary part does not lie within the contour γ). Furthermore, we note that this approximation neglects the coupling between the direction cosines $m_1(t)$ and $m_2(t)$. Nevertheless, such a coupling, in addition to the 14 month Chandler wobble, results in a long term wobble around the initial rotation axis, characterized by timescale much longer than the ice age timescale of 1 Myr (Mitrovica & Milne 1998; Sabadini & Vermeersen 2004). In the following sections we consider the TPW displacement $m(t)$ defined as

$$m(t) = p\sqrt{m_1^2(t)+m_2^2(t)} \tag{32}$$

with p being $+1$ or -1, respectively whether the instantaneous rotation pole is farther away or closer from the position of the surface load than its initial position. A zero value $m(t)=0$ means that the instantaneous rotation pole is crossing the initial north pole position.

4 READJUSTMENT OF THE EQUATORIAL BULGE: ELASTIC AND VISCOELASTIC LITHOSPHERE

The numerical algorithm described in Section 3 is now used to elucidate the role of the lithosphere, elastic or viscoelastic. We assume that the viscoelastic lithosphere has a very high viscosity $\nu_L = 10^{26}$ Pa s. The lower and upper-mantle viscosities are $\nu_{LM} = 10^{22}$ and $\nu_{UM} = 10^{21}$ Pa s, respectively.

In Fig. 1(a) we compare the time evolution of the Green's function $k_F^T - K^T\,(t)$, with $K^T\,(t)$ being the convolution of tidal gravitational Love number $K^T\,(t)$ with the Heaviside time history $H(t)$,

for the models with the elastic (E, solid line) and viscoelastic (V, dashed line) lithospheres. It expresses how fast the rotational equatorial bulge readjusts to a new rotation axis. As discussed above in Section 2, we choose for the tidal fluid limit k_F^T, the tidal isostatic response (Chinnery 1975) which are $k_{F,E}^T = 0.920$ and $k_{F,V}^T = 0.934$. The difference $k_{F,V}^T - k_{F,E}^T = 0.014$ reflects a difference in equilibrium flattening. The elastic lithosphere carries a finite strength that, instead, the model with the viscoelastic lithosphere does not have, being fully relaxed at large time (i.e. the elastic lithosphere is pre-stressed while the viscoelastic lithosphere is in hydrostatic equilibrium). Note that $k_{F,E}^T - K_E^T\,(t)$ for the elastic lithosphere case (solid line) is always smaller than $k_{F,V}^T - K_V^T\,(t)$ for the viscoelastic case (dashed line). Within 10 Myr, $k_{F,E}^T - K_E^T\,(t)$ approaches zero, namely the equatorial bulge readjusts completely to a new rotation axis. On the contrary $k_{F,V}^T - K_V^T\,(t)$ is 0.014 at 10 Myr, which is precisely the difference between the fluid limits $k_{F,V}^T$ and $k_{F,E}^T$. This indicates that the accumulated stresses during the displacement of the equatorial bulge are almost completely relaxed within the viscoelastic mantle, but they are still present in the viscoelastic lithosphere with high viscosity. Indeed the viscoelastic lithosphere behaves as an elastic one at timescale lower than the lithospheric Maxwell time, 50 Myr. We show this in Fig. 1(b) for the time window of 50 Myr where, in addition to the previous Green's functions, we plot also their difference $k_{F,V}^T - K_V^T\,(t) - (k_{F,E}^T - K_E^T\,(t))$ (dash-dotted line). Before 10 Myr, the Green's functions $K_V^T\,(t)$ and $K_E^T\,(t)$ coincide and the only difference between $k_{F,V}^T - K_V^T\,(t)$ and $k_{F,E}^T - K_E^T\,(t)$ is due to the difference in fluid numbers $k_{F,V}^T - k_{F,E}^T = 0.014$. After 10 Myr this difference reduces since the viscoelastic lithospere relaxes and the rotational bulge readjusts completely to the new rotation axis. Nevertheless, as shown in Fig. 1(a), this process is intermingled with the gravitational overturning due to the unstable compositional stratification of PREM above the 670 km discontinuity (Plag & Jüttner 1995). The unstable compositional C-modes (Cambiotti & Sabadini 2010) make $K^T\,(t)$ change sign. The cuspidal point at $t = 400$ Myr represents, in the logarithmic scale, this change of sign, from positive to negative, of the Green's function $k_{F,V}^T - K^T\,(t)$ for the case with a highly viscous viscoelastic lithosphere. For the elastic lithosphere case, the change of sign of the Green's function $k_{F,E}^T - K_E^T\,(t)$ occurs at 130 Myr. This overturn is a mathematical consequence of the unstable PREM stratification but has little physical consequence as on this long timescale, the TPW is anyway dominated by mantle convection (Spada *et al.* 1992b).

In Fig. 1(c) we compare the time evolution of the Green's function $1 + K^L\,(t)$, with $K^L\,(t)$ being the convolution of load gravitational Love number $K^L\,(t)$ with the Heaviside time history $H(t)$, for the models with the elastic (E, solid line) and viscoelastic (V, dashed line) lithospheres. It expresses the return to isostatic compensation of a surface point-like load. The two load Green's functions agree up to 10 Myr, but after this time $1 + K_V^L\,(t)$ goes to zero for the viscoelastic lithosphere case as the load becomes fully isostatic compensated. Instead, $1 + K_E^L\,(t)$ for the elastic lithosphere case converges to the value of 0.0102, which is the gravitational anomaly $1 + k_{F,E}^L$ remaining because of the elastic support. In the end, starting from 1 Gyr, the gravitational overturn breaks the final equilibrium with the load, the cuspidal points at 2.3 and 1.3 Gyr for the elastic and viscoelastic lithosphere cases, respectively, having the same meaning as in Fig. 1(a).

These findings show that over the timescale of postglacial rebound and until 10 Myr as well, there are no significant differences between the tidal, $K^T\,(t)$ and load, $K^L\,(t)$, Love numbers computed with an elastic lithosphere or with a viscoelastic lithosphere with high viscosity, $\nu_L = 10^{26}$ Pa s. However the TPW involves not only

the Love numbers $K^T(t)$ and $K^L(t)$ at short time period but also the limit at infinite time of the tidal Love number $K^T(t)$, the so-called tidal fluid limit k_F^T, as seen in eq. (16). As $k_{F,V}^T \neq k_{F,E}^T$, the rheology of the lithosphere, elastic (E) or viscoelastic (V, i.e. fluid at infinite time), controlling the equilibrium figure of the Earth (see also fig. 1 in Mitrovica *et al.* 2005), does affect the TPW. Thus, models with elastic and viscoelastic lithospheres do not lead to the same TPW. The equilibrium figures are different for the two cases and the rotation of the model with the highly viscous viscoelastic lithosphere is more stable since its equatorial bulge is not able to readjust to a new rotation axis on the ice age timescale (Mitrovica *et al.* 2005). From Figs 1(a) and (b), we can understand that the sensitivity on the lithospheric rheology, pointed out by Nakada (2002), actually is due to the stabilizing effects of delay of the readjustment of the hydrostatic equatorial bulge. Classically, the lower mantle viscosity ν_{LM} was considered as the main parameter controlling this delay.

Instead, adopting Earth models with the highly viscous viscoelastic lithosphere, as rightly suggested by Mitrovica *et al.* (2005), allows to take into account also the delay associated with the high lithospheric viscosity ν_L, in addition to that associated with the lower mantle viscosity ν_{LM}.

5 COMPRESSIBLE AND INCOMPRESSIBLE LOVE NUMBERS

The incompressible Maxwell Earth models have been widely used in the last two decades for TPW simulations. For this reason we now compare these models with the compressible Maxwell Earth models. At the same time, we quantify the effects of the different rheologies of the lithosphere, elastic or viscoelastic.

Fig. 2 shows the comparison between the compressible (solid line) and incompressible (dashed line) Green's functions
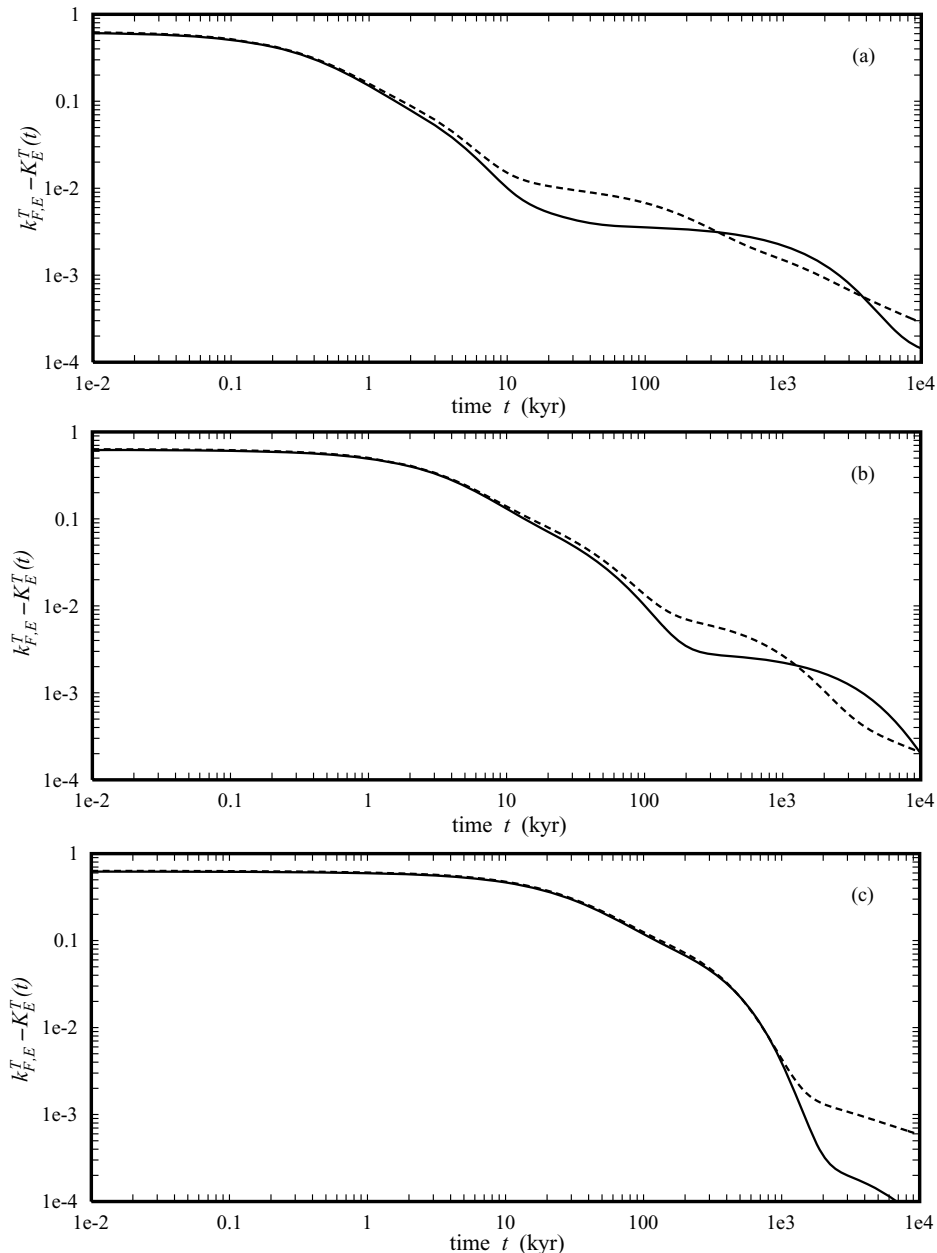

Figure 2. The readjustment of the equatorial bulge $k_{F,E}^T - K_E^T(t)$ for the compressible (solid) and incompressible (dashed) PREM with the elastic (E) lithosphere. The lower mantle viscosity is $\nu_{LM} = 10^{21}$ (a), $\nu_{LM} = 10^{22}$ (b) and $\nu_{LM} = 10^{23}$ (c) Pa s.
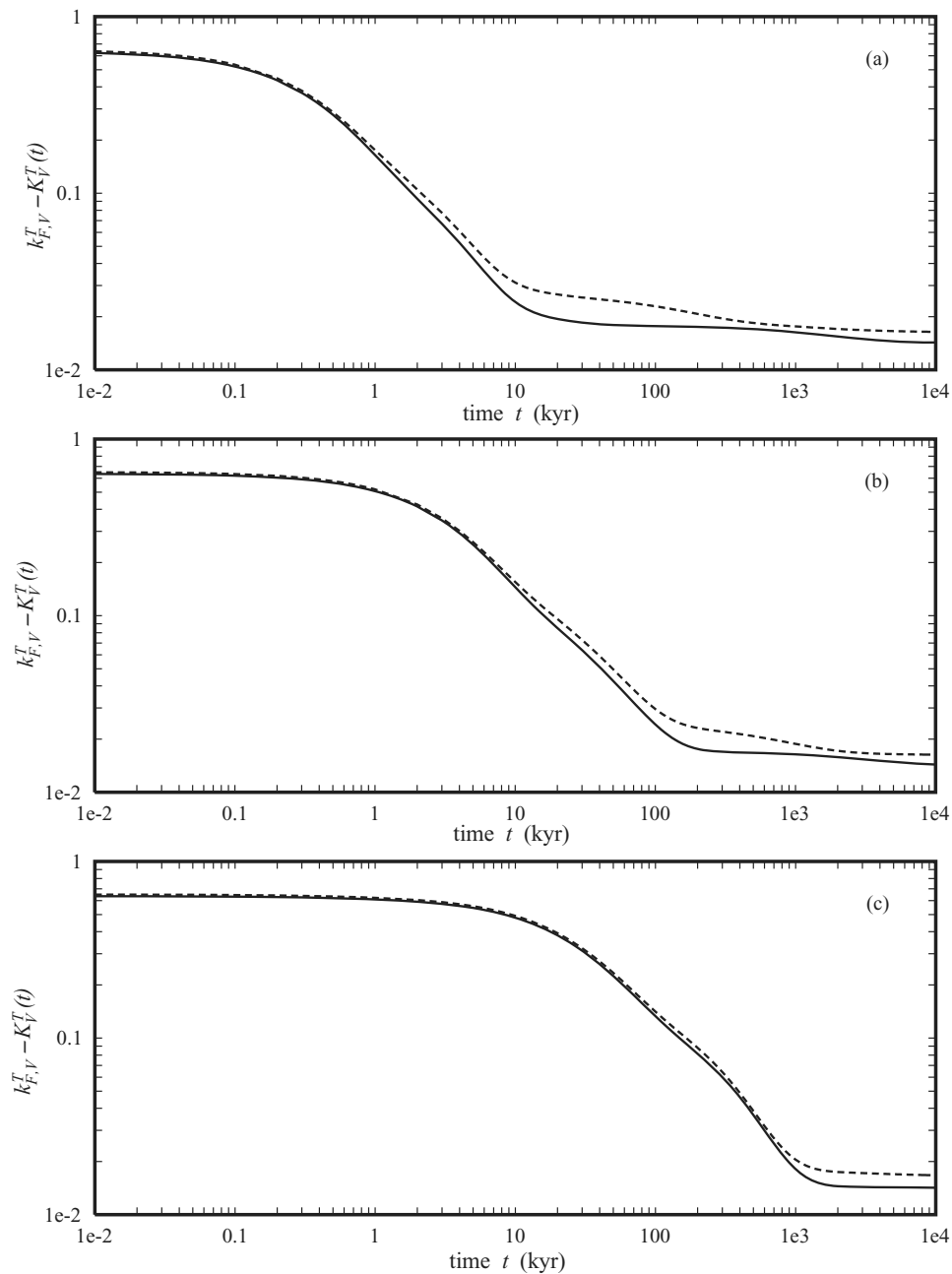
Figure 3. The readjustment of the equatorial bulge $k^T_{F,V} - K^T_V(t)$ for the compressible (solid) and incompressible (dashed) PREM with the viscoelastic (V) lithosphere, $\nu_L = 10^{26}$ Pa s. The lower mantle viscosity is $\nu_{LM} = 10^{21}$ (a), $\nu_{LM} = 10^{22}$ (b) and $\nu_{LM} = 10^{23}$ (c) Pa s.

$k^T_{F,E} - K^T_E(t)$ in the case of an elastic (E) lithosphere, 120 km thick. The lower mantle viscosity ν_{LM} is increased by one order of magnitude from 10^{21}, 10^{22} to 10^{23} Pa s from top to bottom panel. The time window considered is 10 Myr, much longer than the ice age timescale of 1 Myr. In general the compressible rotational bulge readjusts faster than the incompressible one, the Green's function $k^T_{F,E} - K^T_E(t)$ for the compressible model being lower than that for the incompressible model, with the exception of the time intervals $[3 \times 10^2, 4 \times 10^3]$ kyr (panel a) and $[10^3, 10^4]$ kyr (panel b) for the lower mantle viscosities $\nu_{LM} = 10^{21}$ and 10^{22} Pa s, respectively. For $\nu_{LM} = 10^{23}$ Pa s (panel c) the two models predict very similar values until 1 Myr, where the compressible rotational bulge begins to readjust faster to the new rotation axis than the incompressible one.

In Fig. 3, the elastic (E) lithosphere has been replaced by the viscoelastic (V) lithosphere, with $\nu_L = 10^{26}$ Pa s. In this case, the Green's function $k^T_{F,V} - K^T_V(t)$ for the compressible model is always lower than that for the incompressible model. The vertical scale has been reduced compared to Fig. 2. Indeed, at 10 kyr, all the layers have significantly relaxed except for the highly viscous viscoelastic lithosphere, which behaves as an elastic one as shown in Fig. 1(b). This results in the fact that at 10 Myr both the compressible and incompressible Green's functions $k^T_{F,V} - K^T_V(t)$ differ from zero by the discrepancy $k^T_{F,V} - k^T_{F,E}$. Since $k^T_{F,E}$ depends on the rheology of the elastic lithosphere, compressible, 0.920, or incompressible, 0.918, the discrepancy $k^T_{F,V} - k^T_{F,E}$ for the compressible model, 0.014, is smaller than that for the incompressible model, 0.016. Thus, before 10 Myr, the viscoelastic compressible lithosphere is
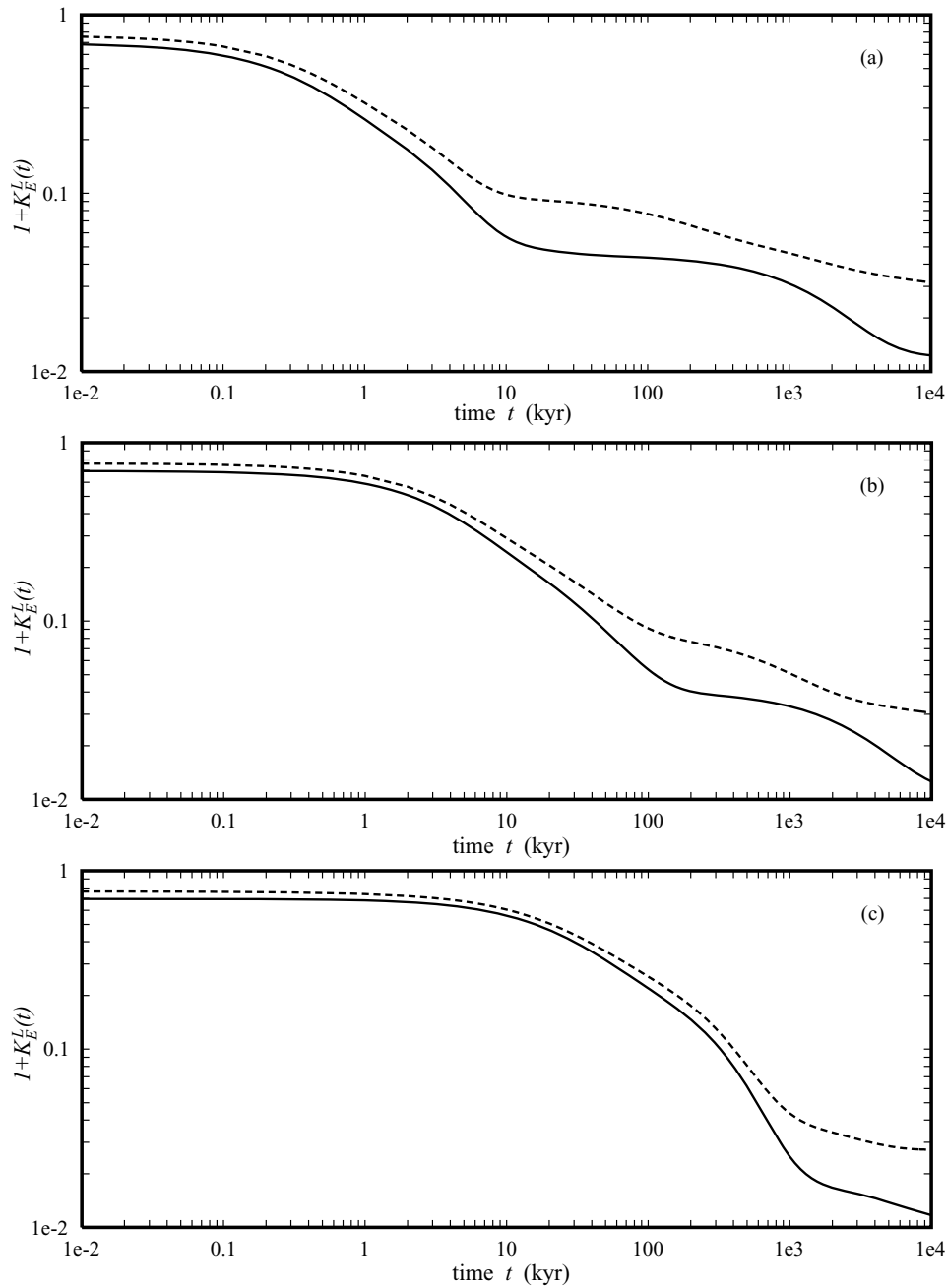
Figure 4. Load response $1 + K_E^L(t)$ of the compressible (solid) and incompressible (dashed) PREM with the elastic (E) lithosphere. The lower mantle viscosity is $\nu_{LM} = 10^{21}$ (a), $\nu_{LM} = 10^{22}$ (b) and $\nu_{LM} = 10^{23}$ (c) Pa s.

more deformable than the incompressible one and this explains the fact that the compressible Green's function $k_{F,V}^T - K_V^T(t)$ is smaller than the incompressible one.

Fig. 4 shows the comparison between the compressible (solid line) and incompressible (dashed line) Green's function $1 + K_E^L(t)$ for the elastic (E) lithosphere case. As in Figs 2 and 3, the lower mantle viscosity ν_{LM} is increased by one order of magnitude from 10^{21} to 10^{23} Pa s in each panel and we consider a time window of 10 Myr. The Green's function $1 + K_E^L(t)$ for the compressible model is always lower than for the incompressible models, indicating that compressible models are more deformable. The difference between the compressible and the incompressible cases is larger for the load response than for the equatorial bulge readjustment (compare

Fig. 4 with Figs 2 and 3). Particularly, in the elastic limit $t \to 0$, the readjustment of the equatorial bulge is marginally affected by the different rheologies (see Figs 2 and 3), while compressible and incompressible cases differ by 10 per cent for loading, Fig. 4. We do not show the results for the model with the viscoelastic lithosphere since, on the timescale of 10 Myr, they are very similar to those shown in Fig. 4 for the elastic lithosphere case.

By comparing the Green's functions between the panels of Figs 2, 3 and 4, we note that the increase of the lower mantle viscosity ν_{LM} by one order of magnitude, from 10^{21} (panels a) to 10^{23} (panels c) Pa s, delays by one order of magnitude the time at which compressibility becomes effective during the transient, from 10 to 10^3 kyr, both for loading and equatorial bulge readjustments. This makes
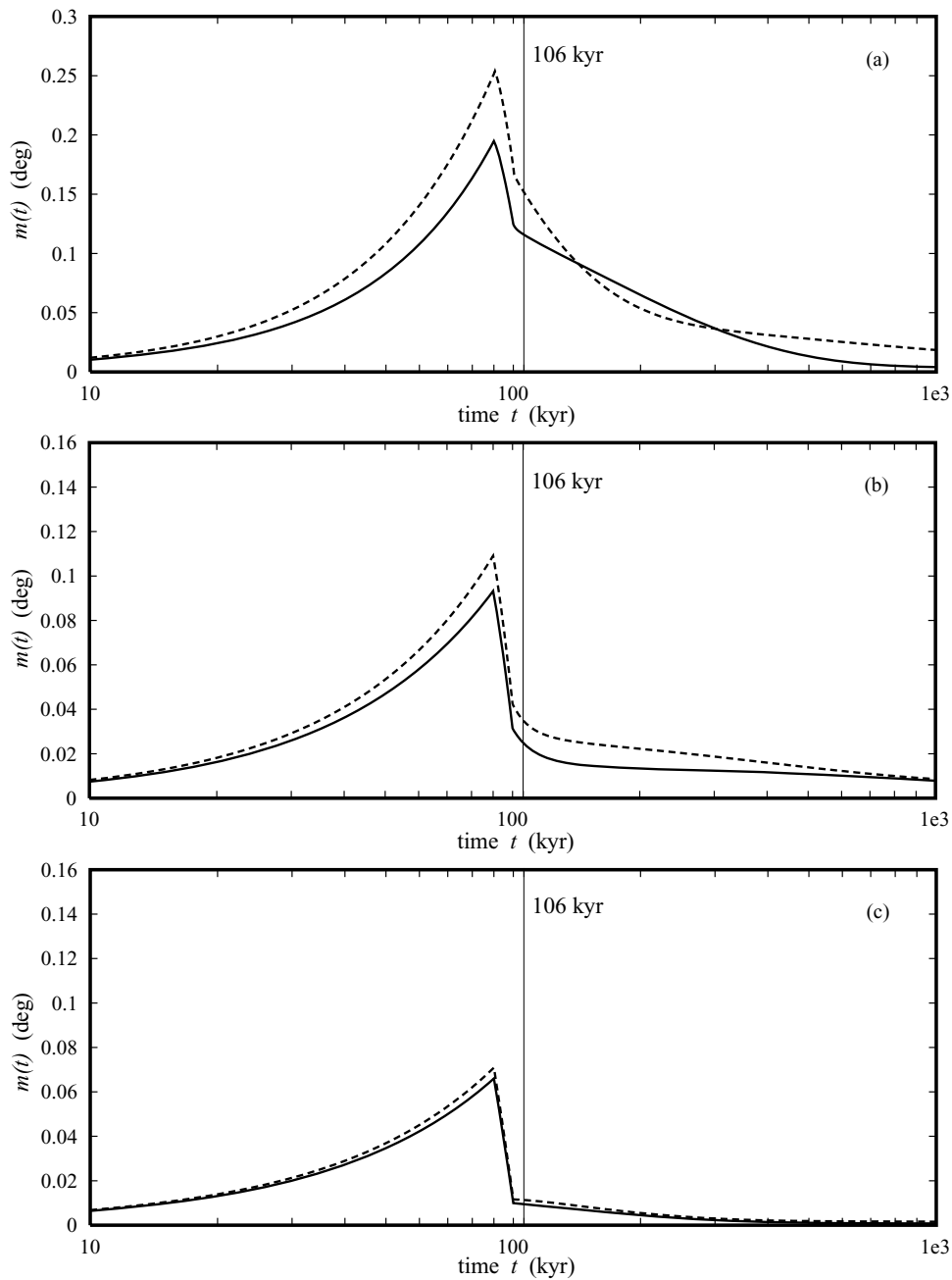
Figure 5. The TPW displacement $m(t)$ due only to the last ice age for the compressible (solid) and incompressible (dashed) PREM with the elastic lithosphere. The lower mantle viscosity is $\nu_{LM} = 10^{21}$ (a), $\nu_{LM} = 10^{22}$ (b) and $\nu_{LM} = 10^{23}$ (c) Pa s.

compressibility almost undistinguishable from incompressibility on timescale of the ice ages, 1 Myr, for the high lower mantle viscosity $\nu_{LM} = 10^{23}$ Pa s (panels c).

6 COMPRESSIBLE AND INCOMPRESSIBLE TRUE POLAR WANDER

Once these Green's functions are introduced into the linearized rotation equations, the pole displacement $m(t)$, eqs (31) and (32), can be computed. For the ice loading, we consider only the last ice age, characterized by linear glaciation and deglaciation phases of 90 kyr and 10 kyr and the same maximum ice sheet inertia pertur-

bations as in Mitrovica *et al.* (2005), $\Delta_{13}^{ice} = -6.67\,10^{31}$ kg m^2 and $\Delta_{23}^{ice} = 2.31\,10^{32}$ kg m^2. Figs 5 and 6 compare the TWP displacements $m(t)$ for compressible (solid line) and incompressible (dashed line) models with the elastic and the viscoelastic lithospheres, both without considering any non-hydrostatic contribution from mantle convection that will be discussed later. As for Figs 2, 3 and 4, the TPW displacements are computed for increasing lower mantle viscosities ν_{LM}, from 10^{21} (panels a) to 10^{23} Pa s (panels c).

The shape of TPW displacement curves is characterized by an increasing displacement during the glaciation phase, from 10 to 90 kyr, away from Hudson bay followed by a still ongoing displacement toward Hudson Bay. Starting from the elastic lithosphere results, Fig. 5, the TPW displacements for the compressible models are
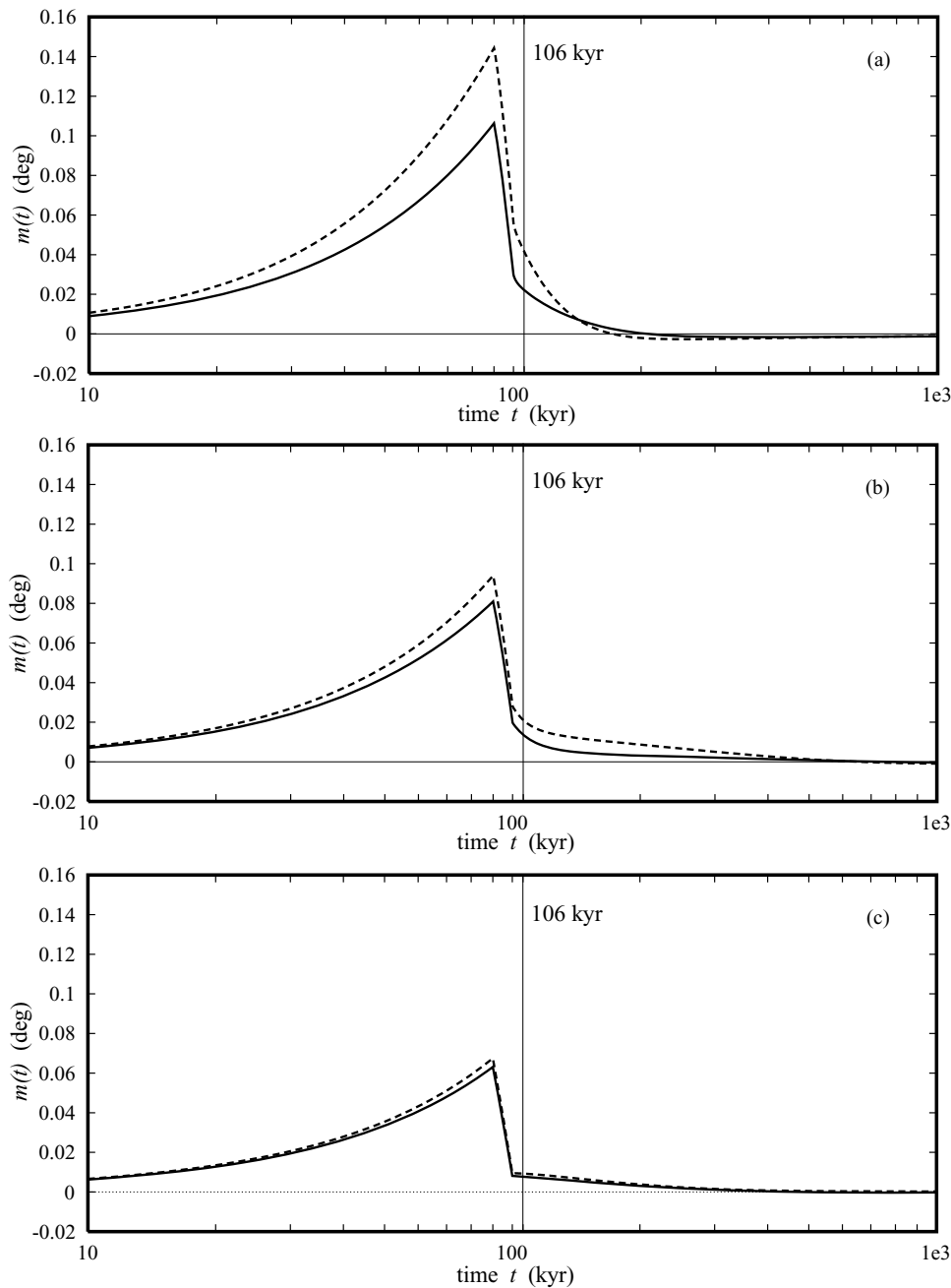
Figure 6. The TPW displacement $m(t)$ due only to the last ice age for the compressible (solid) and incompressible (dashed) PREM with the viscoelastic lithosphere, $v_L = 10^{26}$ Pa s. The lower mantle viscosity is $v_{LM} = 10^{21}$ (a), $v_{LM} = 10^{22}$ (b) and $v_{LM} = 10^{23}$ (c) Pa s. The negative values of $m(t)$ indicate that the rotation pole has already crossed its initial position.

always smaller than those for the incompressible ones, except when $v_{LM} = 10^{21}$ Pa s (panel a) in the time interval [120, 200] kyr. This finding is in agreement with the Green's functions $1 + K_E^L(t)$ of Fig. 4, illustrating that the incompressible lithosphere does not readjust to a load as fast as the more deformable compressible one and thus the ice age loading drives more efficiently the polar wander for the incompressible rheology.

As already observed from the Green's functions, an increase of the lower mantle viscosity v_{LM} reduces the differences between the compressible and incompressible models, as clearly shown in Fig. 5(c). The TPW displacements are always positive, meaning that the rotation pole never crosses the initial north pole while it

moves back towards Hudson bay. Indeed the displacements $m(t)$ at $t = 1$ Myr differ significantly from the initial north pole position at zero, particularly for lower mantle viscosities 10^{21} and 10^{22} Pa s, Figs 5(a) and (b), and for the incompressible rheology. This shows that each glaciation cycle moves the pole by a finite amount away from Hudson bay not only for the layered incompressible models as the secular term of eq. (28) implies, but also for continuous, compressible or incompressible, models.

The models with the viscoelastic lithosphere are depicted in Fig. 6. The TPW displacements resemble those shown in Fig. 5 for the case of the elastic lithosphere, although with some reduction in amplitudes. This behaviour is more effective for the lower mantle

viscosity $\nu_{LM} = 10^{21}$ Pa s, characterized by almost a factor of 2 reduction (compare panels (a) of Figs 5 and 6). This indicates that the difference between the viscoelastic lithosphere and the elastic one is the largest for a soft lower mantle. Differently from Fig. 5, now the rotation pole crosses the initial north pole at about 200 kyr, Fig. 6(a) and at 700 kyr, Fig. 6(b), both for compressible and incompressible models, while for the lower mantle with high viscosity, Fig. 6(c), the crossing occurs at 500 kyr only for the compressible model. Thus the TPW displacement of models with a viscoelastic lithosphere does not end up with any finite displacement away from Hudson bay (Mitrovica *et al.* 2005). This drastic reduction of the TPW displacement is due to the increased delay in the readjustment of the hydrostatic equatorial bulge due to the highly viscous viscoelastic rheology of the lithosphere which stabilizes rotationally the planet, as discussed in Sections 4 and 5.

The drastic reduction of the TPW displacement when the viscosity of the viscoelastic lithosphere is reduced to that of the upper mantle, $\nu_L = 10^{21}$ Pa s, compared to the elastic case, has been shown first in Vermeersen & Sabadini (1999), Fig. 8, for the full series of ice age cycles. In this case, two counteracting effects are involved. First, the easier relaxation of the lithospheric stresses accumulated during the polar excursion allows the equatorial bulge to readjust faster, as pointed in Fig. 3 of Ricard *et al.* (1993b). Second, the full isosatic compensation on the ice age timescale reduces the perturbation of the inertia tensor $\mathbf{J}^L$ due to the ice age loading, eq. (10). Between the two effects, which respectively reduces and increases the rotational stability of the Earth, the stabilizing one due to isostatic compensation is dominant as indicated by the reduction of the TPW displacement. The importance of the full isostatic compensation in TPW predictions can be understood by considering that the viscoelastic lithosphere nullifies the secular term responsible of a net shift of the rotation axis away from Hudson bay after the end of each ice age cycle. Indeed, the load fluid love number being $k_L^F = 1$ for the viscoelastic lithosphere, the factor s can be simplified from the numerator and the denominator of eq. (28).

Although carried out with different values for the lithospheric viscosity ν_L, the viscoelastic TPW calculation of Vermeersen & Sabadini (1999), Nakada (2002), Mitrovica *et al.* (2005) and those given in Fig. 6 behave as expected on the basis of the underlying physical hypotheses. Particularly, the 'Nakada paradox' is explained within the 'traditional approach' in terms of an increase in the delay of the readjustment of the hydrostatic equatorial bulge due to the high lithospheric viscosity ν_L .

7 THE ROLE OF MANTLE HETEROGENEITIES

To estimate the correction β, eq. (22), Mitrovica *et al.* (2005) considers the difference between the observed fluid Love number $k_{F,obs}^T$ and the tidal fluid limit $k_{F,\text{II}}^T$ coming from the second-order theory of the hydrostatic equilibrium figure of the rotating Earth (Nakiboglu 1982). These authors found that $\beta = k_{F,obs}^T - k_{F,\text{II}}^T = 0.008$. This difference represents the non-hydrostatic contribution due to the lateral density variations and dynamic topography sustained by convection.

Nakiboglu's hydrostatic flattening is close to the values given by other authors (Denis 1989; Alexandrini 1989). However as the β parameter is the small difference between two large numbers (observed fluid Love number and tidal fluid limit), the β deduced from these different authors only agree within 10 per cent. Note also that all these papers were using PREM (Dziewonski & Anderson

1981) which was in agreement with an Earth's mass and inertia that have been sligthly reevaluated since. The hydrostatic flattening according to Clairaut's first-order theory is essentially controlled by I/Ma^2 (Radau's result, where I, M and a are the Earth's inertia, mass and radius), a parameter equal to 0.3308 in PREM while the most recent estimate is 0.33069 (Chambat & Valette 2001). This reevaluation should reduce the predicted hydrostatic flattening and, by consequence, increase β. Clearly a more rigorous estimate of the hydrostatic flattening is needed but is beyond the goal of this paper (see Chambat *et al.* 2010). It seems qualitatively that the β parameter chosen by Mitrovica *et al.* (2005) might be a conservative value that could be increased up to $\beta = 0.01$. Mitrovica *et al.* (2005) were aware of the possible uncertainty on the β parameter and indeed they consider the reasonable range $0.006 < \beta < 0.01$ in their Fig. 10.

We now quantify the effects of the slow mantle convection for models with a highly viscous viscoelastic lithosphere, $\nu_L = 10^{26}$ Pa s, by making use of the same β correction as in Mitrovica *et al.* (2005), namely $\beta = 0.008$ in eq. (21). Fig. 7 shows the effects of this non-hydrostatic contribution to the equatorial bulge, to be compared with Fig. 6. For the soft lower mantle $\nu_{LM} = 10^{21}$ Pa s (panels a of Figs 6 and 7), the minor differences during the active loading glaciation–deglaciation phase, from 10 to 100 kyr, are accompanied by large deviations at the end of the unloading. At 100 kyr, the displacement is reduced by a factor of 3 with respect to the compressible rheology and almost by a factor of 2 with respect to the incompressible one. For the higher lower mantle viscosities $\nu_{LM} = 10^{22}$ Pa s (panels b) and $\nu_{LM} = 10^{23}$ Pa s (panels c), the effects of the non-hydrostatic contribution are not as important. The TPW displacement for $\nu_{LM} = 10^{21}$ Pa s is so inhibited by the non-hydrostatic contribution that both compressible and incompressible models predict a change of sign in the displacement $m(t)$ at about 15 kyr after the end of deglaciation, Fig. 7(a), with the axis of rotation being displaced toward the deglaciated region with respect to the initial north pole. Zero crossings occur earlier in time also for the higher viscosity cases, Figs 7(b) and (c), but not as dramatically as for the models with the soft lower mantle of $\nu_{LM} = 10^{21}$ Pa s.

This behaviour of the TPW displacement, like a dampened pendulum crossing the initial north pole, occurs both for the high lithospheric viscosity and in the presence of a non-hydrostatic correction β. It is a completely different process than that due to the coupling in the linearized rotation equations of the direction cosines $m_1(t)$ and $m_2(t)$ involved by the first term of the right side of eqs (16) and (23), neglected in the present work following Mitrovica & Milne (1998). This coupling explains the 14 month Chandler wobble and a small amplitude wobble with a period much larger than the 1 Myr considered in Figs 6 and 7.

We now investigate the sensitivity of the present-day TPW predictions to the rheology of the lithosphere and to the β correction. Fig. 8 shows the present-day TPW rate, namely the time derivative of the displacements of Figs 5, 6 and 7 evaluated at 6 kyr after the end of unloading, as a function of the lower mantle viscosity ν_{LM}. We use the compressible model with a viscoelastic lithosphere (dashed line) and we vary the β correction (thin solid lines) by steps of 0.002 from 0.002 to 0.016, around the value of 0.008 (dash-dotted line) used in Mitrovica *et al.* (2005). The case with an elastic lithosphere is indicated by the thick solid line. In this figure, only one ice cycle is considered. The largest sensitivity of TPW rates to lithospheric rheology and β correction occurs for lower mantle viscosities ν_{LM} smaller than 10^{22} Pa s. At $\nu_{LM} = 10^{21}$ Pa s the predicted rates vary from -0.91 deg Myr^{-1}, for the model with the elastic lithosphere (thick solid line), to -0.29 deg Myr^{-1}, for the model with
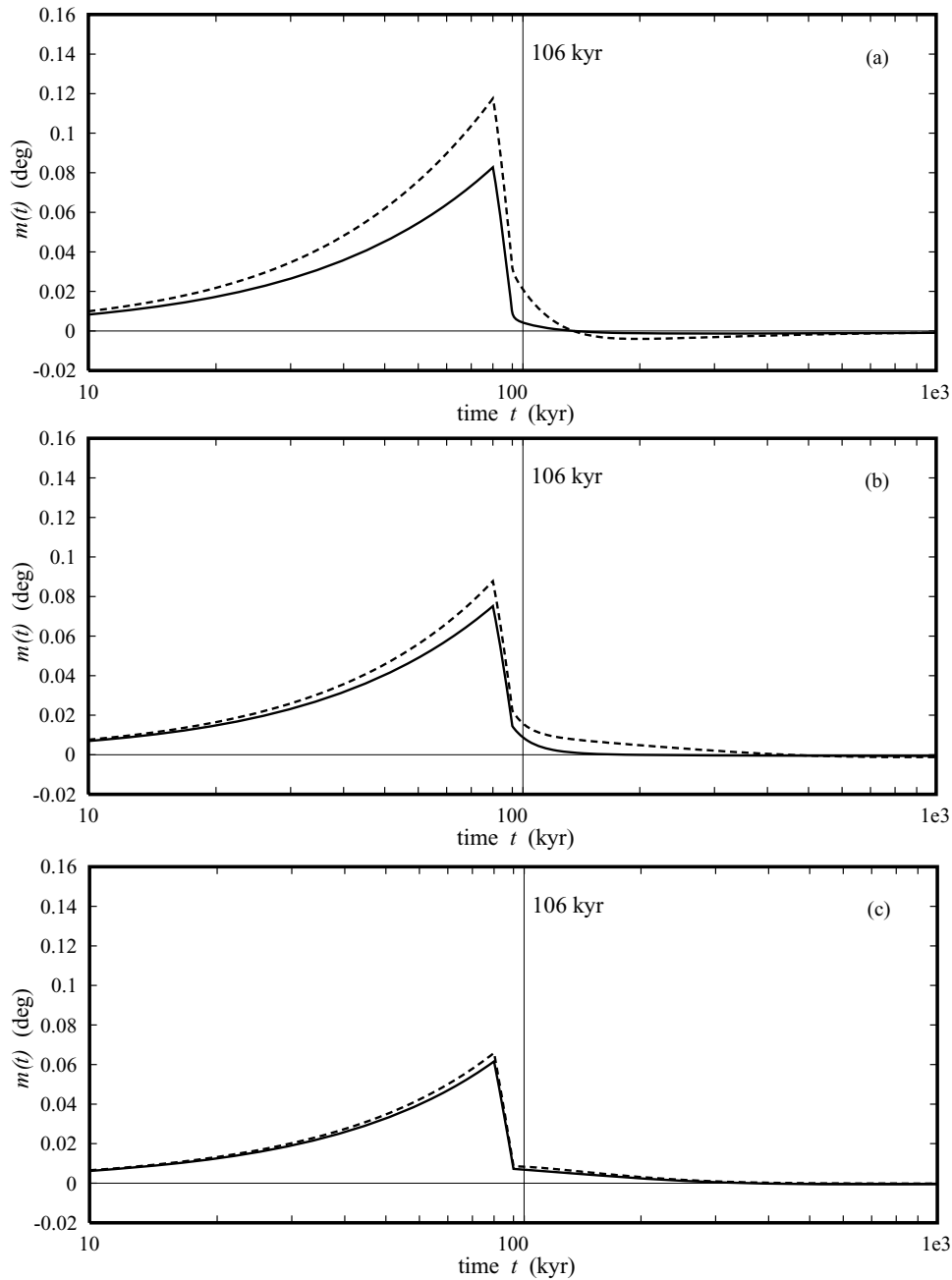
Figure 7. The TPW displacement $m(t)$ due to the last ice age only of the compressible (solid) and incompressible (dashed) PREM with the viscoelastic lithosphere, $\nu_L = 10^{26}$ Pa s and the non-hydrostatic correction $\beta = 0.008$. The lower mantle viscosity is $\nu_{LM} = 10^{21}$ Pa s (a), $\nu_{LM} = 10^{22}$ Pa s (b) and $\nu_{LM} = 10^{23}$ Pa s (c). The negative values of $m(t)$ indicate that the rotation pole has already crossed its initial position.

the viscoelastic lithosphere and the correction $\beta = 0.008$ (dash-dotted line). As first shown by Mitrovica *et al.* (2005), the effects of the non-hydrostatic bulge is to dampen TPW rates when the lower mantle viscosity ν_{LM} is in the range [10^{21}, 10^{22}] Pa s. For very large β corrections, 0.014 and 0.016, the damping effect of the non-hydrostatic bulge is made evident by the change of sign of the TPW rate, indicating that the rotation pole crosses its initial position and is going now away from Hudson bay once again. The non-hydrostatic contribution from convection is so effective in fixing the rotation axis that the pole of rotation comes back to its initial position without any finite displacement of the pole.

A better comparison with Mitrovica *et al.* (2005) results and a more realistic estimate of present-day TPW rates, is obtained by considering the full series of eight ice age cycles, as shown in Fig. 9. For the elastic lithosphere case and when $\nu_{LM} = 10^{21}$ Pa s, adding the seven previous ice age cycles to the single one of Fig. 8, increases the TPW rates by a factor of 2, while for ν_{LM} greater than 10^{22} Pa s the increase is only of 10 per cent or less. On the contrary, for the model with the viscoelastic lithosphere, both with or without the non-hydrostatic contribution, the previous seven ice ages have a negligible effect, the differences being lesser than 5 per cent for the whole range of lower mantle viscosity. This
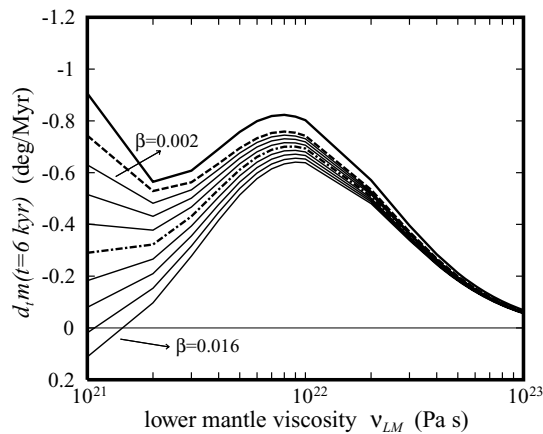
Figure 8. The present TPW rate $d_t m(t)$ due only to one ice age, evaluated at 6 kyr after the end of the deglaciation, as function of the lower mantle viscosity ν_{LM}, for PREM with the elastic lithosphere (thick solid line), the high viscosity viscoelastic lithosphere, (dashed line), $\nu_L = 10^{26}$ Pa s and with the non hydrostatic contribution $\beta = 0.008$ (dashed-dot line). The thin solid lines refer to the PREM with the highly viscous viscoelastic lithosphere and the non-hydrostatic correction β varying from 0.002 to 0.016 by steps of 0.002, from top to bottom. The sign of $d_t m(t)$ indicates whether the rotation pole moves forward to, negative, or go away from, positive, the Hudson bay.
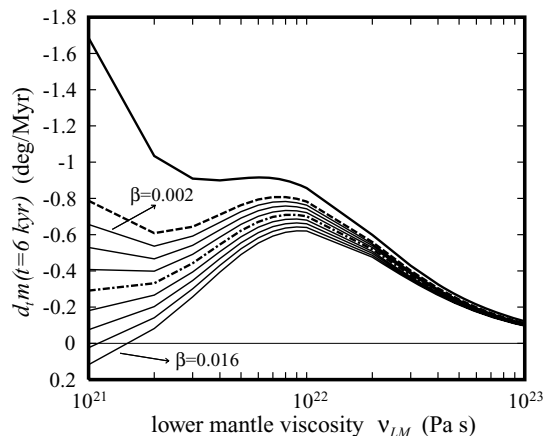

Figure 9. The same as Fig. 8, but for the full series of eight ice ages.

shows that the TPW rate remains mostly sensitive to only the last ice age.

This latter remark explains also why, with the elastic lithospheric rheology, the TPW rate versus lower mantle viscosity ν_{LM} does not have the same bell shape as the geopotential changes due to PGR. In this case, the TPW predictions are sensitive also to the previous seven ice ages mainly for lower mantle viscosity in the range of $[10^{21}, 10^{22}]$ Pa s as it results from the comparison of Figs 8 and 9 for the model with the elastic lithosphere (thick solid lines). This is due to the fact that, without a highly viscous viscoelastic lithosphere or a non-hydrostatic contribution from mantle convection, the only stabilizing effect is the delay in the readjustment of the hydrostatic equatorial bulge to the axis of instantaneous rotation controlled by the lower mantle viscosity ν_{LM}, which becomes smaller and smaller decreasing ν_{LM}.

The damping effect due to the high viscosity of the lithosphere and to the non-hydrostatic contribution is more evident in the displacement of the rotation axis than in the TPW rate, as we show in Fig. 10. After the eight ice age cycles, in the case of the elastic

lithosphere (thick solid line), the axis of rotation is displaced from its initial position by 0.27 deg, at $\nu_{LM} = 10^{21}$ Pa s, and this value diminishes gradually with the lower mantle viscosity to about 0.02 deg Myr^{-1} at $\nu_{LM} = 10^{23}$ Pa s. The rheology change from elastic (thick solid line) to viscoelastic (dashed line) lithosphere causes reductions in the TPW displacements by factors ranging from 20, at $\nu_{LM} = 10^{21}$ Pa s, to 2, at $\nu_{LM} = 10^{23}$ Pa s. The value obtained for our compressible model with the elastic lithosphere and the low lower mantle viscosity of $\nu_{LM} = 10^{21}$ Pa s is very similar to what is obtained in Vermeersen & Sabadini (1999) for a simpler 5-incompressible model. The TPW displacements are subjected to further reductions when a β correction is added. Particularly, for $\beta = 0.008$ (dash-dotted line), the rotation pole crosses the initial north position. Generally, as shown in Fig. 10(b), the TPW displacements for the viscoelastic lithosphere range in a narrow interval of $[-0.011, 0.022]$ deg for any values of the lower mantle viscosity ν_{LM}, even without the β correction.

The present-day TPW rates obtained by using the correction $\beta = 0.008$ reaches at most -0.71 deg Myr^{-1} for a lower mantle viscosity $\nu_{LM} = 8 \times 10^{21}$ Pa s. This is -0.29 deg Myr^{-1} lower than the observed rate of -1 deg Myr^{-1}. Our findings fully support the results obtained by Mitrovica *et al.* (2005) and, having been obtained on the basis of compressible Earth models which take into account continuous variations of the material parameters and thus relying on the contour integration rather than on normal mode summation, they provide an independent confirmation. Even if we consider models with elastic lithosphere we obtain the same TPW predictions once the tidal fluid limit $k_{F,E}^T = 0.920$ from modelling is replaced by the estimate $k_{F,obs}^T = 0.942$ of Mitrovica *et al.* (2005), their eq. (16). Indeed the stabilizing effect of the larger non-hydrostatic bulge for models with elastic lithosphere, $\beta = k_{F,obs}^T - k_{F,E}^T = 0.022$, would be quantitatively the same of the two stabilizing effect acting in the case of models with the highly viscous viscoelastic lithosphere: the delayed readjustment of the equatorial bulge together with the smaller non-hydrostatic bulge, $\beta = k_{F,obs}^T - k_{F,V}^T = 0.008$. This means that TPW studies cannot discriminate between the effects of the lithospheric rheology and of the lateral density variations and dynamic topography sustained by convection. In any case, the parameter β has to be consistent with mantle convection models.

8 CONCLUSIONS

We have compared ice age TPW predictions using the traditional approach where the equilibrium flattening is self consistently computed (Sabadini & Peltier 1981; Sabadini *et al.* 1982; Wu & Peltier 1984) and the scheme proposed by Mitrovica *et al.* (2005) where the observed tidal fluid number is considered. The motion of the rotation axis, given by the linearized Liouville eq. (16), depends on the load-induced perturbation, $1 + \tilde{k}^L(s)$ and on the readjustment of the equatorial bulge, $k_F^T - \tilde{k}^T(s)$. Over the time of ice ages, the load, $\tilde{k}^L(s)$ and tidal, $\tilde{k}^T(s)$, Love numbers, computed for models with an elastic and highly viscous viscoelastic lithosphere are the same. Nevertheless, the traditional approach leads to different TPW predictions due to the fact that the highly viscous viscoelastic lithosphere implies an extra delay of the readjustment of the equatorial bulge, compared to the elastic lithosphere (see Fig. 1). The elastic and viscoelastic lithospheres are indeed associated with different stress patterns. Frozen stresses are present in the elastic lithosphere before and after the glaciation, while the viscoelastic lithosphere is initially stress free and it builds up stress that cannot relax during the polar motion for high lithospheric viscosities.
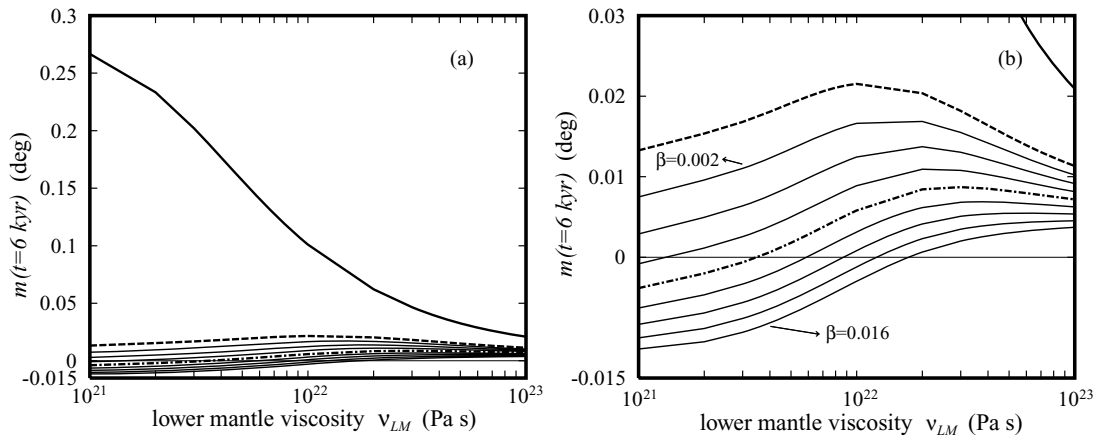
Figure 10. The present TPW displacement $m(t)$ due to the full series of eight ice ages, evaluated at 6 kyr after the end of the deglaciation, as function of the lower mantle viscosity ν_{LM}, for PREM with the elastic lithosphere (thick solid line), the high viscosity viscoelastic lithosphere, (dashed line), $\nu_L = 10^{26}$ Pa s and with the non-hydrostatic correction $\beta = 0.008$ (dashed-dot line). The thin lines refer to PREM with the viscoelastic lithosphere and the non-hydrostatic correction β varying from 0.002 to 0.016 by steps of 0.002, from top to bottom. The negative values of $m(t)$ indicates that the rotation pole has already crossed its initial position. The panel (b) shows the enlargement of the panel (a) in the range of $[-0.015, 0.03]$ deg.

To take into account the difference between observed and modelled tidal fluid numbers, Mitrovica *et al.* (2005) introduce the β-correction, eq. (22). This scheme represents a first attempt to couple mantle convection with ice age TPW within a linear rotation theory. As first enlightened by Mitrovica *et al.* (2005), this ice age-convection coupling dampens present-day ice age TPW rates since the non-hydrostatic extra bulge, frozen within the planet, stabilizes the planet by slowing down the displacement of the axis of rotation away from this fixed orientation so effectively that the rotation pole goes back to its initial position at large time. We show that self-consistent non-hydrostatic bulge resulting from convection calculations plays a fundamental role in obtaining realistic estimates of this non-hydrostatic contribution, due to its major impact in TPW simulations in the $[10^{21}, 10^{22}]$ Pa s lower mantle viscosity range.

With the extra degree of freedom given by the parameter β, models with elastic and highly viscous elastic lithosphere lead to the same ice age TPW prediction. It is therefore difficult to choose the most appropriate lithospheric rheology when the distinction is made between the actual shape of the Earth and its equilibrium shape. We agree however with Mitrovica *et al.* (2005) that using a viscoelastic lithosphere in the framework of the traditional theory seems reasonable because it is simpler (but not necessary true) to start from a relaxed lithospheric stress and because the tidal fluid limit from the viscoelastic modelling is closer to observation and thus a smaller mantle contribution β needs to be introduced.

The present-day value of β, related to the excess flattening due to mantle convection, cannot be best evaluated than by subtracting the computed hydrostatic tidal fluid limit to the observed fluid Love number, eq. (22). On geological timescale, as the Earth is constantly reorienting to maximize its equatorial inertia, that is, to be more flattened than the hydrostatic estimate, β should always remain positive except maybe during exceptional inertial interchange polar excursion (Richards *et al.* 1999). The value of the non-hydrostatic contribution β due to convection can be estimated by means of convection models or, for the last hundred million years, from paleoreconstruction of plate tectonics Ricard *et al.* (1993a). The difference between the time dependent inertia terms remains of the same order than Mitrovica *et al.* (2005) estimate of 0.008 within a factor 2. This means that the Earth's rotation axis is always very stable with respect to short term forcings like glaciations: as soon as the forcing

vanishes, the mantle anomalies force the rotation axis to come back to its initial position. Only mantle convection can drive large TPW displacements (Spada *et al.* 1992b).

Once the Mitrovica *et al.* (2005) estimate of the correction $\beta = 0.008$ is taken into account, the highest present-day TPW rate of 0.71 deg Myr^{-1} from glacial forcing is obtained for a lower mantle viscosity of 10^{22} Pa s, which means that at least 30 per cent of the observed value of 1 deg Myr^{-1} remains unexplained. This implies that mantle convection must drive polar motion to be compliant with observations. Recent mantle circulation models by Schaber *et al.* (2009), characterized by a large heat flux at the core–mantle boundary, require a lower mantle viscosity of 10^{23} Pa s to stabilize the planet rotation, leading to TPW rates of about 0.5 deg Myr^{-1} in rough agreement with the direction towards Newfoundland in the last 100 Myr. The first self-consistent TPW calculations from mantle convection have been obtained by Ricard *et al.* (1993b) and already required a substantial increase in the lower mantle viscosity, 10^{22} Pa s at least, to rotationally stabilize the planet. The ice age TPW, coupled with the stabilizing effect of the excess flattening due to mantle convection, in addition to the TPW driven by mantle convection are thus both needed to fulfill observations, requiring lower mantle viscosity ranging from 10^{22} to 10^{23} Pa s. If this is the case, the β-correction proposed by Mitrovica *et al.* (2005) would only impact marginally the estimate of ice age TPW rates, as it would be the high viscosity of the lower mantle that would control the TPW. It is notable that an inconsistency for lower mantle viscosity predictions between glacial and convection forcing continues to exist. Indeed, for the Schaber *et al.* (2009) estimate of 10^{23} Pa s lower mantle viscosity, glacial forcing would provide at most TPW rates of 0.1 deg Myr^{-1} that, summed to the convection TPW rate of 0.5 deg Myr^{-1}, would not explain the observation of 1 deg Myr^{-1}. The exact balance of the TPW, between deglaciation and convection forcings, is therefore not yet well understood.

Chambat and Maria Chiara Bianchi for their help in the estimate of the non-hydrostatic bulge.

REFERENCES

Alessandrini, B., 1989. The hydrostatic equilibrium figure of the Earth - an interative approach, *Phys. Earth Planet. Inter.,* **54,** 180–192.

Besse, J. & Courtillot, V., 1991. Revised and synthetic apparent polar wander paths of the African, Eurasian, North American, and Indian Plates, and true polar wander since 200 Ma', *J. geophys. Res.,* **96,** 4029–4050.

Cambiotti, G. & Sabadini, R., 2010. The compressional and compositional stratifications in Maxwell Earth models: the gravitational overturning and the long period tangential flux, *Geophys. J. Int.,* **180,** 475–500, doi:10.1111/j.1365-246X.2009.04434.x

Cambiotti, G., Barletta, V.R., Bordoni, A. & Sabadini, R., 2009. A comparative analysis of the solutions for a Maxwell Earth: the role of the advection and buoyancy force, *Geophys. J. Int.,* **176,** 995–1006, doi:10.1111/j.1365-246X.2008.04034.x.

Chambat, F. & Valette, B., 2001. Mean radius, mass, and inertia for reference Earth models, *Phys. Earth Planet. Inter.,* **124,** 237–253.

Chambat, F., Ricard, Y. & Vallette, B., 2010. Flattening of the Earth: further from hydrostaticity than previously estimated, *Geophys. J. Int.,* **183,** 727–732, doi:10.1111/j.1365-246X.2010.04771.x.

Chinnery, M.A., 1975. The static deformation of an earth with a fluid core: a physical approach, *Geophys. J. R. astr. Soc.,* **42,** 461–475.

Denis, C., 1989. The hydrostatic figure of the Earth, in *Gravity and Low Frequency Geodynamics* (chap. 3), *Physics and Evolution of the Earth's Interior,* **Vol. 4,** ed. Teisseyre, R., Elsevier, Amsterdam.

Dziewonski, A.M. & Anderson, D.L., 1981. Preliminary reference Earth model, *Phys. Earth Planet. Inter.,* **25,** 297–356.

Fang, M. & Hager, B.H., 1995. The singularity mystery associated with a radially continuous Maxwell viscoelastic structure, *Geophys. J. Int.,* **123,** 849–865.

Han, D. & Wahr, J., 1995. The viscoelastic relaxation of a realistically stratified earth, and a further analysis of postglacial rebound, *Geophys. J. Int.,* **120,** 278–311.

Jeffreys, M., 1952. *The Earth,* Cambridge Univ. Press, Cambridge.

Mitrovica, J.X. & Milne, G.A., 1998. Glacial-induced perturbations in the Earth's rotation: a new appraisal, *J. geophys. Res.,* **103,** 985–1005.

Mitrovica, J.X., Wahr, J., Matsuyama, I. & Paulson, A., 2005. The rotational stability of an ice-age earth, *Geophys. J. Int.,* **161,** 491–506, doi:10.1111/j.1365-246X.2005.02609.x.

Munk, W.H. & MacDonald, G.J.F., 1960. *The Rotation of the Earth: A Geophysical Discussion,* Cambridge University Press, London, New York, Melbourne.

Nakada, M., 2002. Polar wander caused by the Quaternary glacial cycles and fluid Love number, *Earth Planet. Sci. Lett.,* **200,** 159-166, doi:10.1111/j.1365-246X.2005.02609.x.

Nakiboglu, S.M., 1982. Hydrostatic theory of the Earth and its mechanical applications, *Phys. Earth planet. Int.,* **28,** 302–311.

Plag, H.-P. & Jüttner, H.-U., 1995. Rayleigh-Taylor instabilities of a self-gravitating Earth, *J. Geodyn.,* **20,** 267–288.

Ricard, Y., Richards, M.A., Lithgow-Berteloni, C. & Le Stunff, Y., 1993a. A geodynamic model of mantle mass heterogeneities, *J. geophys. Res.,* **98,** 21 895–21 909.

Ricard, Y., Spada, G. & Sabadini, R., 1993b. Polar wandering of a dynamic Earth, *Geophys. J. Int.,* **113,** 284–298.

Richards, M., Bunge, H.P., Ricard, Y. & Baumgardner, J.R., 1999. Polar wandering and inertial interchange events in mantle convection models, *J. Geophys. Lett.,* **26,** 1777–1780.

Sabadini, R. & Vermeersen, L.L.A., 2004. *Global Dynamics of the Earth: Applications of Normal Mode Relaxation Theory to Solid-Earth Geophysics,* 1st edn, Kluwer Academic Publisher, Dordrecht, Boston, London.

Sabadini, R. & Peltier, W.R., 1981. Pleistocene deglaciation and the Earth's rotation: implication for mantle viscosity, *Geophys. J. R. astr. Soc.,* **66,** 553–578.

Sabadini, R., Yuen, D.A. & Boschi, E., 1982. Polar wandering and the forced responses of a rotating, multilayered, viscoelastic planet, *Geophys. J. Int.,* **87,** 2885–2903.

Schaber, K., Bunge, H.P. & Schubert, B.S.A., Malservisi, R. & Horbach, A., 2009. Stability of the rotation axis in high-resolution mantle circulation models: weak polar wander despite strong core heating, *Geochem. Geophys. Geosyst.,* **10,** Q11W04, doi:10.1029/2009GC002541.

Smylie, D.E. & Manshina, L., 1971. The elastic theory of dislocations in real earth models and changes in the rotation of the earth, *Geophys. J. R. astr. Soc.,* **23,** 329–354.

Spada, G., Sabadini, R., Yuen, D.A. & Ricard, Y., 1992a. Effects on postglacial rebound from the hard rheology in the transition zone, *Geophys. J. Int.,* **109,** 683–700.

Spada, G., Ricard, Y. & Sabadini, R., 1992b. Excitation of True Polar Wander by subduction, *Nature,* **360,** 452–454.

Tanaka, Y., Okuno, J. & Okubo, S., 2006. A new method for the computation of global viscoelastic post-seismic deformation in a realistic Earth model (I) - vertical displacement and gravity variation, *Geophys. J. Int.,* **164,** 273–289, doi:10.1111/j.1365-246X.2005.02821.x.

Vermeersen, L.L.A. & Sabadini, R., 1999. Polar Wander, sea-level variations and Ice Age cycles, *Surv. Geophys.,* **20,** 415–440.

Vermeersen, L.L.A. & Mitrovica, J.X., 2000. Gravitational stability of spherical self-gravitating relaxation models, *Geophys. J. Int.,* **142,** 351–360.

Vermeersen, L.L.A., Sabadini, R. & Spada, G., 1996. Compressible rotational deformation, *Geophys. J. Int.,* **129,** 735–761.

Vermeersen, L.L.A. & Sabadini, R., 1997. A new class of stratified viscoelastic models by analytical techniques, *Geophys. J. Int.,* **129,** 531–570.

Wu, P. & Peltier, W.R., 1982. Viscous gravitational relaxation, *Geophys. J. R. astr. Soc.,* **70,** 435–485.

Wu, P. & Peltier, W.R., 1984. Pleistocene deglaciation and the Earth's rotation: a new analysis, *Geophys. J. R. astr. Soc.,* **76,** 753–791.

APPENDIX A

Following Tanaka *et al.* (2006), the not-analytic set $\mathcal{S}$ has to be situated on the real axis $\mathbb{R}$ of the Laplace s-domain. However, their result holds only for the part of $\mathcal{S}$ due to the zeros s_j of the secular determinant $\Delta(n, s)$ (eq. 19 in Tanaka *et al.* 2006). We will refer to this set as $\mathcal{S}_0$. In addition $\tilde{\mathbf{k}}(s, n)$ is also not analytic in the not uniformly Lipschitzian intervals $\mathcal{N}$ of the differential system describing the conservation of the momentum and the self-gravitation as pointed out in Fang & Hager (1995) and Cambiotti & Sabadini (2010)

$$\mathcal{N} = \{0\} \cup \mathcal{N}_\tau \cup \mathcal{N}_\varsigma \tag{A1}$$

where

$$\mathcal{N}_\tau = \{s \in \mathbb{C} \,|\, s = -\tau(r) \quad \text{with } r \in [r_C, a]\} \tag{A2}$$

$$\mathcal{N}_\varsigma = \{s \in \mathbb{C} \,|\, s = -\varsigma(r) \quad \text{with } r \in [r_C, a]\}, \tag{A3}$$

with τ and ς being the inverse Maxwell and compressional relaxation times (eq. 15 in Cambiotti & Sabadini 2010). Contrary to the set $\mathcal{S}_0$, the set $\mathcal{N}$ is not associated with the zeros s_j of the secular determinant $\Delta(n, s)$. It is interesting to notice that, $\Delta(n, s)$ being an analytic function in the Laplace s-domain with the exception of the set $\mathcal{N}$, the zeros $s_j \in \mathbb{R} - \mathcal{N}$ have to be isolated and at most denumerable, with cluster points belonging to the boundary of $\mathcal{N}$. Thus, the Love number $\tilde{\mathbf{k}}(n, s)$ has two different types of not analyticity. The first comes from a denumerable set of poles s_j, which are due to the fact that the solution of momentum and Poisson equations has to satisfy, at the same time, both the fluid-solid boundary condition (Chinnery 1975) at the core–mantle interface and the Earth's surface boundary condition describing the forcing. The second comes from the continuous set of inverse Maxwell and compressional relaxation
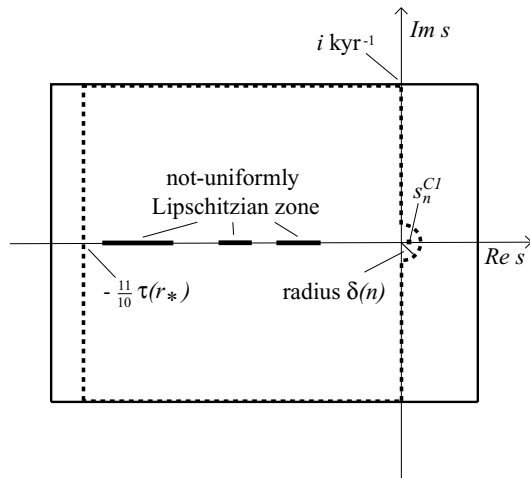
Figure A1. The contour integral γ (dashed line) and that used in Tanaka *et al.* (2006).

times τ and ς. Accordingly to Fang & Hager (1995), we will refer to these contributions as the modal and non-modal contributions, respectively.

The non-modal contribution is inherently associated with the continuous variations of the elastic shear and bulk moduli and of the viscosity. In particular, this constitutes a qualitative difference between continuous Maxwell Earth models, which takes into account the continuous variations of the material parameters, and layered Maxwell Earth models, which take the material parameter constant within each layer. As discussed in Spada *et al.* (1992a), Han & Wahr (1995), Vermeersen & Sabadini (1997) and Cambiotti *et al.* (2009), the τ and ς do not contribute to the perturbations in the time domain, if they are isolated points in the Laplace s-domain, while we have verified that a not null contribution comes from the continuous set $\mathcal{N}$. In any case, this is more a mathematical problem rather than a physical one. Indeed, as discussed in Tanaka *et al.* (2006), the perturbations of very fine layered models converges to those of continuous models if a sufficiently high number of layers is considered.

Fig. A1 shows the contour γ (dashed line) that we use in eq. (30) and the contour of Tanaka *et al.* (2006) (solid line). The difference consists in the fact that our contour γ is situated on the half space with positive real part of the Laplace variable s, $\Re s > 0$, only for

the semi-circle of radius $\delta(n)$ depending on the harmonic degree n

$$\delta(n) = \max\left\{5\, s_n^{C1},\ 10^{-5}\,\mathrm{kyr}^{-1}\right\} \qquad (A4)$$

with s_n^{C1} being the pole of the first unstable C-modes, with overtone number $m = 1$, due to the unstable compositional stratification of the PREM above the 670 km discontinuity (Cambiotti & Sabadini 2010). The factor 5 and the lower bound $10^{-5}\,\mathrm{kyr}^{-1}$ in eq. (A4) have been chosen to avoid numerical unstability in radial Gill–Runge–Kutta integration near s_n^{C1} and $s = 0$, respectively. This choice reduces the numerical unstability in the numerical evaluation of eq. (30) due to the term $e^{\Re s\, t}$, which diverges in the limit $t \to \infty$ if $\Re s > 0$. The pole s_n^{C1} is obtained by a root-finding algorithm, which can be applied safety in the positive half of the real axis since the not uniformly Lipschitzian zone $\mathcal{N}$ is situated in the negative half, by definition, eq. (A1).

The value z_1 defining the lowest $\Re s < 0$ of the contour γ is chosen as

$$z_1 = -\frac{11}{10}\,\tau(r_*) \qquad (A5)$$

with $r_* \in [r_C, a]$ being the radius at which the inverse Maxwell relaxation time τ assumes its greatest value. This is due to the fact that the not analytic set $\mathcal{S}$ can be composed only of isolated poles $s_j \in \mathcal{S}_0$, if $\Re s < -\tau(r_*)$ and our experience has shown that there are not poles such that $s_j < -\tau(r_*)$.

We choose $1\,\mathrm{kyr}^{-1}$ for the greatest and lowest $\Im s$ of the contour γ. Increasing the time t numerical instabilities may happen due to the sign oscillations of $e^{\Im s\, t}$ near the imaginary axis, for small $\Re s$. Indeed, elsewhere the term $e^{\Re s\, t}$ goes rapidly to zero increasing t, since $\Re s < 0$ and this damps the oscillations of $e^{\Im s\, t}$. To avoid the numerical unstability near the imaginary axis, particularly for those s with $\Re s \geq 0$, we proceed as follows. We adopt an adaptive Cavalieri–Simpson method to evaluate the contour integral entering eq. (30) and, at each stage, we increase artfully the sampling of the integrand $\tilde{\mathbf{k}}(n, s)\, f(s)$ by using the same second-order polynomial interpolation on which the Cavalieri–Simpson method is based. This way the number of steps at which $\tilde{\mathbf{k}}(n, s)$ is effectively evaluated depends only on the smoothness or stiffness of $\tilde{\mathbf{k}}(n, s)$ along γ, rather than on the condition $t\,\Im s \ll 2\pi$ proposed by Tanaka *et al.* (2006). The timescale at which the numerical unstability due to the oscillation of $e^{\Im s\, t}$ occurs is increased of about 1-2 orders of magnitude, under the same number of effective evaluations of $\tilde{\mathbf{k}}(n, s)$.